Applied Geochemistry 146 (2022) 105465

Contents lists available at ScienceDirect

Applied Geochemistry

journal homepage: www.elsevier.com/locate/apgeochem

Detection and quantification of low levels of carbonate mineral species using thermogravimetric-mass spectrometry to validate CO_2 drawdown via enhanced rock weathering

Simon J. Kemp [a,*], Amy L. Lewis [b], Jeremy C. Rushton [a]

[a] British Geological Survey, Environmental Science Centre, Keyworth, Nottingham, NG12 5GG, UK
[b] Leverhulme Centre for Climate Change Mitigation, Department of Animal and Plant Sciences, University of Sheffield, Sheffield, S10 2TN, UK

ARTICLE INFO

Editorial handling by Kersten

Keywords:
CO_2
Basalt
Climate change
Modelling
Calcite
Strontianite

ABSTRACT

Enhanced rock weathering (ERW) is a promising technology being actively investigated to ameliorate anthropogenic climate change. ERW accelerates atmospheric carbon dioxide (CO_2) drawdown in agricultural soils following the addition of crushed, silicate rocks. The application of basalt, an abundant silicate rock, has widely been proposed for ERW. In order to measure and model the efficacy of ERW, it is critical to fully characterise the mineralogical composition of the basaltic materials being deployed in laboratory to catchment scale experiments.

As previously demonstrated on analogous basaltic rock and soil materials on Mars, thermal analytical methods such as coupled thermogravimetric analysis-mass spectrometry (TGA-MS), provide a potentially rapid, effective technique to identify and also quantify the carbonate mineral species present in ERW basalts and their weathering products.

Our study of six different basaltic materials used in ERW experiments, from widely different geological and geographical settings, suggests that TGA weight losses can provide useful information on the low-levels of carbonate minerals present. Furthermore, carbonate mineral identification and quantification derived from the accompanying MS-detected CO_2 evolution and corroborated by SEM-EDS mapping, is capable of detecting even lower concentrations with detection limits below 100 ppm for calcite. TGA-MS therefore offers significant advantages over the traditionally-applied inorganic carbon analyses.

Carbonate mineral weight losses encountered during TGA and their accompanying CO_2-evolutions have previously been ascribed to relatively small, defined temperature ranges. However, crucially, this study has revealed the concentration-dependent, large-scale variation in the mass spectrometric peak CO_2-evolution for a range of carbonate minerals. A knowledge of such parameters is imperative for the accurate interpretation of basalt TGA-MS output, the characterisation of these materials and assessment of ERW technologies.

1. Introduction

It is now widely accepted that the anthropogenic emission of greenhouse gases, including carbon dioxide (CO_2), increases atmospheric heat absorption and is responsible for inducing global warming (Myhre et al., 2013). The 2015 Paris Agreement, signed by over 100 countries, adopted the scientific advice of the Intergovernmental Panel on Climate Change (IPCC) and agreed to restrict future warming to within 2 °C of pre-industrial levels, and ideally below 1.5 °C (United Nations Framework Convention on Climate Change, 2015).

While a dramatic reduction in CO_2 emissions is imperative to curb climate change (IPCC, 2014, 2021), the removal of an additional 2–10 Gt of atmospheric CO_2 per yr is predicted to be required to curb anthropogenic global warming (Rockström et al., 2017; Mercure et al., 2018). An array of different techniques for extracting CO_2 from the atmosphere (negative emission technologies, NETs) is being actively investigated to assess their ability to mitigate and ameliorate climate change in terms of feasibility, cost and acceptability (Beerling, 2017; Minx et al., 2018; Fuss et al., 2018; Nemet et al., 2018). These range from afforestation and reforestation, biochar and soil carbon sequestration (SCS), ocean fertilisation, bioenergy with carbon capture and sequestration (BECCS), direct air capture (DAC) and enhanced rock weathering (ERW) (Minx et al., 2017; The Royal Society and Royal Academy of Engineering, 2018; IPCC et al., 2021).

* Corresponding author.
E-mail address: sjk@bgs.ac.uk (S.J. Kemp).

https://doi.org/10.1016/j.apgeochem.2022.105465
Received 10 June 2022; Received in revised form 13 September 2022; Accepted 13 September 2022
Available online 18 September 2022

ERW is a land-based NET strategy which addresses multiple UN Sustainable Development Goals (Smith et al., 2019) and involves amending agricultural soils with crushed abundant silicate rocks (particularly basalt and other mafic rocks) to accelerate carbon capture (Kohler et al., 2010; Hartmann et al., 2013; Taylor et al., 2016; Kelland et al., 2020) (Fig. 1). Natural weathering processes, largely controlled by climate and vegetation, decompose silicate minerals, releasing cations (particularly Ca and Mg), a portion of which reacts with and sequesters atmospheric CO_2. Such weathering processes tend to be faster in tropical environments due to warmer climates, extensive rooting systems and ubiquitous root-associating symbiotic fungi (Taylor et al., 2009). The captured CO_2, in the form of stable bicarbonate ions either (under some circumstances) precipitates as pedogenic carbonate, or is flushed into rivers and transported to the oceans, where it is stored (on human timescales) as bicarbonate ions or potentially permanently as carbonate minerals (Edwards et al., 2017).

Consequently, ERW has the potential to not only lower atmospheric CO_2 but also create an increased, alkaline land-ocean flux that might ameliorate ocean acidification (Hartmann et al., 2013; Taylor et al., 2016; Vakilifard et al., 2021). ERW may also improve the productivity of agricultural land as a soil amendment by buffering soil pH (Swoboda et al., 2022), reducing nitrogen loss (Blanc-Betes et al., 2021) and releasing essential plant nutrients (Kantola et al., 2017; Beerling et al., 2018; Kelland et al., 2020). Possible disadvantages of ERW include increased greenhouse gas emissions resulting from rock milling and transport (Lefebvre et al., 2019), the potential introduction of toxic elements to agricultural soils, biodiversity and water quality impacts and the expansion of the necessary mining and infrastructure (Edwards et al., 2017).

In order to research the potential and consequences for the deployment of ERW on tropical agricultural land, extensive experimental trials and carbon cycle modelling are required at laboratory to catchment scales (e.g. Beerling, 2017; Strefler et al., 2018; Lefebvre et al., 2019; Kelland et al., 2020; Lewis et al., 2021).

Mineralogical characterisation of the applied silicate materials, the host soils and reacted products forms a vital part of all these experiments and is a critical input parameter for geochemical models, used to predict dissolution rates and CO_2 removal potential (Lewis et al., 2021). As detailed above, Ca/Mg silicate weathering represents a sink for atmospheric CO_2, e.g.:

$$CO_2 + 2H_2O + CaAl_2Si_2O_8 = Al_2Si_2O_5(OH)_4 + CaCO_3 \quad (1)$$

However, the weathering of carbonates in the applied silicate materials or host soils does not involve a net loss of atmospheric CO_2 because CO_2 taken up by carbonate weathering is soon returned to the atmosphere following oceanic carbonate precipitation (Berner, 1992; Thorley et al., 2014) e.g.:

$$CaCO_3 + CO_2 + H_2O = Ca^{2+} + 2HCO_3^- \quad (2)$$

Moreover, carbonate weathering may represent a net source of CO_2 if weathered by an agent not derived from atmospheric CO_2, including nitric and sulphuric acids derived from anthropogenic atmospheric pollution or from nitrogen fertilizers (Thorley et al., 2014).

Carbonate minerals are much more reactive than silicate minerals and different carbonate mineral species have varied dissolution rates (Palandri and Kharaka, 2004) which in turn will impact on rates of CO_2 removal. Understanding the nature and quantity of carbonate minerals present, often at low levels, is therefore critical to properly account for the actual silicate-derived cation flux and ultimately to help predict the long-term CO_2 removal potential of ERW at a larger scale (Bach et al., 2019; Lewis et al., 2021).

Carbonate-bearing species (most commonly calcite ($CaCO_3$), dolomite ($CaMg(CO_3)_2$), magnesite ($MgCO_3$), ankerite ($CaMgFe(CO_3)_2$) and siderite ($FeCO_3$)) are routinely identified and quantified in rocks and soils using techniques such as powder X-ray diffraction (XRD), examination using optical or scanning electron microscopy (SEM) or via chemical digestion (calcimeter) for Total Inorganic Carbon (TIC) analyses. However, the lowest possible detection limits afforded by XRD for such species are typically of the order of 0.1 wt% (1000 ppm), depending on the nature of the matrix (e.g. Kemp et al., 2016). Optical and scanning electron microscopy requires the prior preparation of thin sections or polished blocks, and although recent image analysis-based software routines enable non-attended analysis, these are still relatively expensive and time consuming. Quantification via acid dissolution (either H^+ consumption or CO_2 production) suffers due to H^+ consumption with non-carbonate components leading to significant underestimates of carbonate content (e.g. Wang et al., 2012; Pillot et al., 2014). TIC values may also be obtained by leaching with various non-oxidative acids, in order to minimally affect organic carbon, prior to LECO total organic carbon (TOC) analysis. Here samples are combusted in an oxygen atmosphere; any carbon present is converted to CO_2 and detected using a non-dispersive infrared (NDIR) cell. The quantity of CO_2 is converted to %C and subtracted from the total %C from analysis of a non-leached sample to determine the TIC of the sample. The

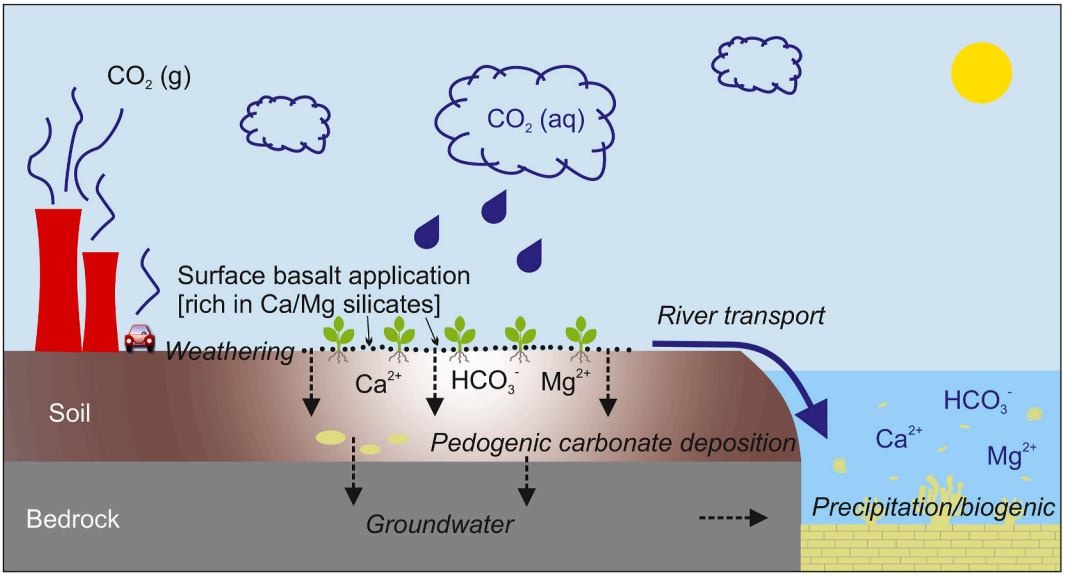

Fig. 1. Enhanced rock weathering in arid climates schematic.

accuracy of such TIC analyses is totally dependent on the questionable, exclusive separation of each type of carbon (TIC v TOC) (Wright and Bailey, 2001). The technique was commonly used for soil and sediment analysis but has now largely been replaced by the more detailed Rock-Eval pyrolysis (e.g. Pillot et al., 2014; Cooper et al., 2021). During Rock-Eval pyrolysis, samples are heated to 300 °C for 3 min, then ramped to 650 °C at a rate of 25 °C min^{-1} in an inert N_2 atmosphere. Any hydrocarbons released during pyrolysis are detected by a flame ionisation detector with an infrared cell detecting the release of CO and CO_2 during the thermal cracking of organic matter.

Thermal analysis techniques, such as coupled thermogravimetric analysis-mass spectrometry (TGA-MS) have the ability to not only rapidly identify but also quantify carbonate species and so complement XRD analysis, particularly where lower levels of detection are required (Charsley et al., 1987; Morgan et al., 1988). For these reasons, thermal analysis instruments have formed an important part of the analytical tools on the Viking, Phoenix and MSL (Curiosity) research missions to Mars (e.g. Sutter et al., 2012, 2017; Archer et al., 2013). In this paper, we highlight the use of TGA-MS for the detection and quantification of low levels of carbonate mineral species in basaltic samples being actively employed in both ERW laboratory experiments and large-scale field demonstrators.

2. Thermal analysis of carbonate minerals

The International Confederation for Thermal Analysis and Calorimetry (ICTAC) defines 'thermal analysis' (TA) as a group of techniques in which a physical or chemical property of a sample is monitored against time or temperature while the temperature of the sample, in a specified atmosphere, is programmed (Hill, 1991). Probably the most common of these techniques are thermogravimetry/thermogravi-metric analysis (TG/TGA) measuring mass, differential thermal analysis (DTA) measuring temperature difference, differential scanning calorimetry (DSC) measuring heat flow and evolved gas analysis (EGA) measuring gases evolved or reacted (Haines, 2002). In order to gain the maximum information about the behaviour of a particular sample, instrumentation may be configured to provide two or more types of measurement at the same time (Simultaneous Thermal Analysis, STA) e.g. TG-DTA, TG-DSC, TG-DTA-EGA.

TA techniques are widely employed across a range of disciplines including chemistry, materials science, foods and pharmaceuticals but are more rarely found in geological/environmental laboratories. However, TA methods frequently provide very useful complimentary data on the mineralogy and behaviour of geological and soil materials (e.g. Morgan, 1977; Morgan et al., 1988; Parsons et al., 1997; Manning et al., 2005).

Carbonate minerals (such as calcite, dolomite, magnesite, strontianite ($SrCO_3$) and witherite ($BaCO_3$)) lend themselves to TA as they decompose via relatively simple, temperature-specific, endothermic reactions (Table 1, Fig. 2). Importantly, Warne (1986) discovered that running carbonate species TA experiments in flowing CO_2, rather than N_2 or air, provided improved individual peak and reaction definition. By adopting the same purge gas as that released during sample decomposition, the carbonate species must overcome the increased CO_2 partial pressure before decarbonation. This 'variable atmosphere thermal analysis' results in increased decomposition temperatures and faster, more vigorous reactions over a smaller temperature range. However, the use of a CO_2 reactive gas negates the possible detection of evolved CO_2 by linked mass spectrometry (MS) or Fourier transform infrared spectrometry (FTIR).

The decarbonation reactions undergone by carbonate minerals are all endothermic but their precise temperature(s) are subject to variation depending not only on instrumental run conditions but also on

Table 1
Carbonate mineral decomposition reactions in flowing N_2 atmosphere (data from Morgan, 1971; Smykatz-Kloss, 1974; Frost et al., 2009; Földvári, 2011).

Carbonate species	Reaction		Temperature range (°C)	Weight loss (%)
	Step	Equation		
Calcite	Total	$CaCO_3 \rightarrow CaO + CO_2$	800–950	43.97
Dolomite	1.	$CaMg(CO_3)_2 \rightarrow CaCO_3 + MgO + CO_2$	600–800	23.48
	2.	$CaCO_3 \rightarrow CaO + CO_2$	800–950	43.97
	Total	$CaMg(CO_3)_2 \rightarrow CaO + MgO + 2CO_2$	600–950	47.77
Magnesite	Total	$MgCO_3 \rightarrow MgO + CO_2$	620–650	52.20
Strontianite (synthetic)	Total	$SrCO_3 \rightarrow SrO + CO_2$	924–1233	29.00
Witherite (synthetic)	Total	$BaCO_3 \rightarrow BaO + CO_2$	800–1300	22.30

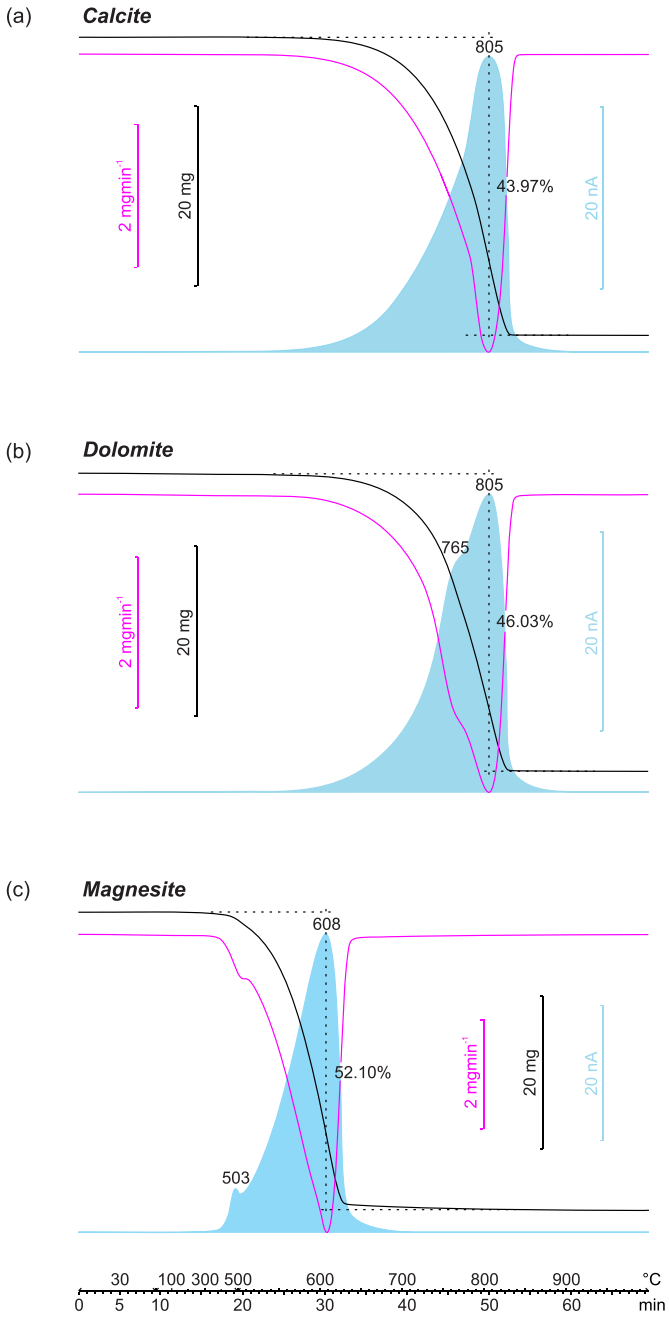

Fig. 2. TGA (black line), DTG (magenta line) and evolved CO_2 profiles (blue integrated area) for (a) calcite, (b) dolomite and (c) magnesite standards. Numerical labels relate to peak maxima on the CO_2 evolution profiles.

differences in particle-size, crystallinity and ionic substitution. Finer particles typically produce a lower temperature onset of dissociation, due to their greater surface area and increased number of broken bonds (Rodriguez-Navarro et al., 2009; Archer et al., 2013). Similarly, smaller crystallite-size distributions also produce lower onset temperatures than larger crystallite-sizes (Földvári, 2011; Pillot et al., 2014). Ionic substitution, typically by other alkaline earth metals, leads to distortion of the crystal lattice and variations in peak temperatures (Frost et al., 2009).

For the present study, we have considered three of the most common carbonate minerals in rocks and soils: calcite, dolomite and magnesite together with two rarer forms: strontianite and witherite, all with end-member compositions. Other carbonate minerals such as ferroan dolomite and ankerite have more variable chemistries as they form part of a solid solution series resulting from Fe^{2+} (with subordinate Mn^{2+}) substituting for Mg^{2+} in the dolomite lattice. Similarly, siderite forms a solid solution series with magnesite and rhodochrosite ($MnCO_3$). Examination of the behaviour of these species was beyond the scope of the present study.

The thermal decomposition of calcite, commonly known as calcining or calcination, has been studied for many years (e.g. Faust, 1950; Boynton, 1980; Rodriguez-Navarro et al., 2009). In inert atmospheres, the peak decarbonation occurs between 800 and 900 °C (Table 1) but samples with smaller crystallite-size distributions show peak temperatures 20–50 °C lower than those samples with larger distributions (Smykatz-Kloss, 1974; Földvári, 2011). Calcite's stoichiometric decarbonation weight loss is 43.97% (Table 1).

Thermal analysis has shown that dolomite decomposes in two stages with maxima at ~800 and ~900 °C (Table 1) (Smykatz-Kloss, 1974; Otsuka, 1986; Engler et al., 1989; Shahraki et al., 2009; Földvári, 2011). As for calcite, both dolomite decomposition temperatures are sensitive to atmospheric CO_2 partial pressure. Increasing the CO_2 partial pressure results in the higher temperature feature shifting to a higher temperature and the lower temperature feature shifting to a lower temperature. Such shifts can be advantageous to the TGA-identification and quantification of dolomite, particularly in the presence of calcite (Kemp et al., 2010). Although, dolomite typically produces a two-stage CO_2 evolution, in an unconfined sample environment and/or at low concentrations, dolomite yields a single CO_2 evolution peak that is indistinguishable from calcite (Milodowski and Morgan, 1980). The theoretical total dolomite decarbonation weight loss is 47.77% (Table 1).

The endothermic decomposition of magnesite occurs at a lower temperature than calcite and dolomite, between 620 and 650 °C, the peak of which decreases with increasing Fe content (Smykatz-Kloss, 1974; Földvári, 2011). Magnesite loses 52.20% of its weight during this decomposition reaction (Table 1).

Two endotherms were noted in the DTA curve of strontianite (Morgan, 1971). The first at 927 °C represents the transition from orthorhombic to hexagonal form and the second peaks at 1233 °C, where dissociation is accompanied by CO_2 release. Dissociation may commence as low as 850 °C (Morgan, 1971). Synthetic strontianite produced a lower dissociation temperature range between 709 and 869 °C, with an expected mass loss of 29.00% (Table 1, Frost et al., 2009).

The high temperature decomposition of witherite has not been so extensively studied as such temperatures were typically beyond the scope of early TGA furnaces. Dissociation begins at ~800 °C with a polymorphic transition from orthorhombic to tetragonal (Frost et al., 2009; Földvári, 2011) and peaks at 1195 °C (Földvári, 2011) with an expected, stoichiometric mass loss of 22.30% (Table 1).

TGA weight losses therefore have excellent potential to rapidly detect and measure low levels of carbonate minerals in geological materials. However, the even greater sensitivity resulting from the addition of MS evolved gas analysis (Haines, 2002; Sutter et al., 2017) offers the potential to detect carbonate minerals at significantly lower levels.

2.1. Detection and quantification

Previous studies have shown that thermal analysis techniques can detect low levels of carbonate minerals in natural or synthetic mixtures. Differential thermal analysis (DTA) using flowing CO_2 detected amounts as low as 0.25% (2500 ppm), a significant improvement over static air DTA (Warne, 1977; Warne and Mitchell, 1979). Later developments suggested that certain carbonates might be detected in the hundreds of ppm concentration range using DTA linked to non-dispersive infrared (NDIR) detectors (Milodowski and Morgan, 1980).

However, over 40 years of technological improvements have helped to further reduce these lower detection limits. The 1970's thermal analysis systems analysed single samples and produced analogue output to paper charts from which peak areas were tediously measured by planimeter (introducing some inaccuracy) and amounts of CO_2 were determined either by empirical calculation or by comparison with standards of known volatile content. Due to the limitations of the equipment of the time (typically 0.1 mg), the 1970s papers also used carbonate minerals mixed with alumina to achieve low concentrations of standard (e.g. Milodowski and Morgan, 1980). This involved significant weighing and homogenisation issues and introduced further errors. Less accurate, faster heating rates (15°C/min) were also employed.

Modern thermal analysis equipment is digital, more accurate (with the best thermobalances now reading to 1e-7 g, 0.0001 mg) and therefore enables the direct weighing of mineral standards, without dilution. Robotic sample changers are routinely specified, enabling continuous analytical runs of batches of, for example, up to 34 samples in the case of the Mettler-Toledo system used in this study, substantially improving laboratory efficiency. Baseline drift, a significant problem in earlier systems, has been eradicated by replacing resistance wound furnaces with, for example infrared heating. Such new technologies maintain excellent temperature control in the balance chamber with fluctuations of less than 0.005 °C measured during ambient to 1200 °C experiments (Dallas, 2006). Exceptional heating rate stability and reproducibility (<0.1%) over the full experimental temperature range has also been demonstrated (Dallas, 2006). Peak areas are now more accurately measured following deconvolution and integration using computer software algorithms. Owing to the small mass analysed, there is a continuing need to ensure sample homogeneity and representivity before TGA (e.g. Robinson et al., 2016).

3. Materials

In order to produce TGA-MS calibration curves, mineral standard samples for the carbonate minerals most likely to be present in the ERW basalts (calcite, dolomite, magnesite, strontianite and witherite) were sourced from the British Geological Survey's internal reference collection. The standards were variously characterised using XRD and geochemical analysis prior to TGA-MS (Table 1S (Supplementary Material)).

Basalts are common, dark-coloured, mafic, finely-crystalline, generally extrusive igneous rocks that typically form as lava flows or small intrusive bodies (USGS, 2015). The International Union of Geological Sciences (IUGS) classify basalts as comprising 45–53% silica (SiO_2) with less than 10% feldspathoid by volume, and where at least 65% of the rock is plagioclase feldspar (Le Bas and Streckeisen, 1991). Basalts may be further sub-divided into alkali basalt and subalkali basalt according to the state of silica saturation (Gillespie and Styles, 1999).

Mineralogically, basalts essentially contain calcic plagioclase feldspar and pyroxene, with or without olivine, often with accessory minerals including magnetite, ulvospinel and ilmenite (Shelley, 1992). Basaltic glass may also form a significant component of a basalt's composition (Allen et al., 1981). The originally-crystallised basalt mineralogy may then undergo modification via relatively high temperature metamorphism, lower temperature hydrothermal alteration and weathering. Carbonate minerals are most commonly formed during

basalt alteration with seawater (e.g. Seyfried and Bischoff, 1974; Alt and Honnorez, 1984; Zhang and Smith-Duque, 2014), groundwater (Möller et al., 2016; Kanakiya et al., 2017) or surface weathering (Gislason et al., 1996; Schaef et al., 2009; Li et al., 2016) and pedogenesis (e.g. Capo et al., 2000; Sayyed, 2014).

A suite of six, globally-relevant basaltic samples, undergoing research as possible ERW materials (Lewis et al., 2021), was selected for this study (Table 2). The samples were sourced from various geographical locations and represent different basalt types and mineral compositions that have subsequently undergone different degrees of metamorphic and weathering alteration (Table 2). As the basalt samples represent quarried fines (suitable for ERW application), these may therefore include 'contaminants' such as other rock fragments (e.g. limestone), soil, or anthropogenic materials (including organic matter). Full details of the mineralogical and geochemical characterisation of the basaltic samples is provided in Lewis et al. (2021). Briefly, however, the basalts formed during crustal extension (Tichum, Hillhouse, Cragmill and Oregon) are composed of greater proportions (46.7–82.0 wt%) of faster weathering minerals (Palandri and Kharaka, 2004), including olivine, augite and plagioclase when compared to those formed at convergent margins (Tawau) which contain a significant proportion (24.9 wt%) of slower weathering minerals such as quartz and clay minerals. The Blue Ridge metabasalt contains a smaller proportion of fast weathering minerals (19.6%) compared to the other samples, as a result of its metamorphic alteration. Fast-weathering basaltic glass forms a significant component (24.9 wt%) of the Oregon basalt.

Typically, basalts are therefore rich in divalent cations and poor in silica (compared to other igneous rocks), usually containing 7–10 wt% Ca, 5–6 wt% Mg and 7–10 wt% Fe which are readily liberated by reaction with CO_2-rich water (Oelkers et al., 2008). The dissolution rate of Mg and Ca is two orders of magnitude greater than reaction with other more crystalline or silica-rich rocks (Wolff-Boenisch et al., 2006).

4. Methods

4.1. Thermogravimetric analysis-mass spectrometry

Representative sub-samples of each mineral standard or basaltic material were ball-milled to <0.125 mm to produce homogeneous powders for analysis. TGA-MS analyses were carried out using a Mettler-Toledo TGA/DSC 3+ thermobalance connected to a Pfeiffer Vacuum ThermoStar mass spectrometer via a heated (150 °C), 0.3 mm OD, quartz capillary. Although the MS offers the ability to measure gases in the range 1–200 amu, only selected gases (H_2O, m/z 18 and CO_2, m/z 44) were monitored for this study. Prior to commencing sample analyses, the TGA/DSC system was calibrated using the manufacturer's specified Indium/Aluminium (In/Al) melting test. Zero runs were then completed for empty 150 μl platinum crucibles. The TGA was controlled and TGA output traces were interpreted using the Mettler-Toledo STAR^e software suite (v16.10). The linked MS was triggered by the TGA but otherwise programmed and MS output displayed using Quadera software (v4.62). Where necessary, overlapping peak areas were deconvolved using PeakFit software (v.4.12). Prior to measurements, the MS was calibrated using the manufacturer's standard procedures to account for drift in the current amplifier, SEM gain and mass scale adjustment.

In order to establish calibration curves and the lower detection limit (LDL) of the different carbonate species, a series of TGA/DSC runs were performed on decreasing amounts of each carbonate species, generally in the range 0.01–75 mg. Samples were accurately weighed directly into 150 μl platinum crucibles using a 5 decimal place Sartorius R200D balance. In addition, to test the LDL, small quantities of calcite standard were added to an inert, milled corundum (American Elements - PN:AL-OY-03-P) matrix and mixed using prolonged reciprocal shaking.

The standard TGA run commenced with a 10 min-isotherm at 30 °C to allow CO_2 levels to decrease and stabilise following opening of the furnace and insertion of the sample crucible. The samples were then subjected to a ramped heating program of 30–500 °C at a heating rate of 50 °C/minute (ramp 1), followed by heating from 500 to 1000 °C at a rate of 10 °C/minute (ramp 2). The analytical run time was ~69 min per sample with ~30 min required to cool the furnace between runs. The faster heating rate of ramp 1 was employed to reduce the analysis time by 28 min per sample, without compromising the detection and quantification of carbonate minerals. The initial isotherm and both ramp stages were completed under N_2 flowing at 40 ml/min, which proved both sufficient to maintain an inert atmosphere, and to quickly escort reaction gases to the mass spectrometer, preventing unwanted secondary reactions. Due to their higher decomposition temperatures, the strontianite and witherite standards were run on an extended program: 10 min-isotherm at 30 °C, 30 to 700 °C at a heating rate of 50 °C/minute (ramp 1) followed by heating from 700 to 1300 °C at a rate of 10 °C/minute (ramp 2).

The presence and quantification of the different carbonate species was determined by comparison with empirically-derived standard weight losses and temperatures (Table 1).

Portions of the ERW basaltic samples (~75 mg) were run on the same standard analytical program and the output interpreted in comparison to the calibration samples.

Table 2
Enhanced rock weathering (ERW) experimental materials. [Contains Data © University of Sheffield].

Locality	Geological setting (age)	Reference	Classification* (Lewis et al., 2021)	LECO analyses (wt%)			Coulometric analyses (wt%)
				TOC	TIC	Equivalent calcite	
Cragmill, Northumberland, UK	Whin Sill (dolerite) emplacement, Pennsylvanian (Carboniferous)	Sabine et al. (1954)	Basalt (TAS) Basalt/andesite (QAPF)	0.013	0.046	0.38	na
Tichum Creek, Queensland, Australia	Associated with continental-mantle plume magmatism (Miocene)	Whitehead et al. (2007)	Basanite (TAS) Phonolitic tephrite (QAPF)	na	na	na	na
Oregon, USA	Prineville Chemical Type Unit, Columbia River Basalt Group. (Middle Miocene)	Smith and Hayman (1987)	Basanite (TAS) Latite (QAPF)	0.015	0.019	0.16	na
Hillhouse, Troon, UK	Intrusive analcime gabbro (Carboniferous–Permian)	Kirstein et al. (2006)	Basalt (TAS) Basalt/andesite (QAPF)	na	na	na	na
Tawau, Sabah, Malaysia	Associated with magmatic-arc volcanism (Pleistocene)	Tahir et al. (2010)	Basaltic andesite (TAS) Dacite (QAPF)	0.013	0.077	0.64	na
Blue Ridge, Illinois, USA	Catocin Greenstone, Virginia, USA (Neo-Proterozoic)	USGS (2019)	Chlorite-actinolite metabasalt (Robertson, 1999)	0.020	0.411	3.43	0.68

Classification schemes*.
TAS: Total Alkaline Silica (Le Bas et al., 1986)
QAPF: Quartz, Alkaline feldspars, Plagioclase feldspars and Feldspathoid (Streckeisen, 1974)

4.2. Scanning electron microscopy

For corroboration of the TGA-MS analyses, further portions of the crushed basaltic samples were mounted and polished in blue-dye-impregnated (to highlight porosity) resin blocks and examined using a Zeiss Sigma 300 field emission scanning electron microscope (SEM). The SEM was fitted with twin Bruker Xflash 6|30, 30 mm^2, 129eV resolution, energy dispersive X-ray (EDX) detectors running with Bruker Esprit (v2) software and Zeiss' Mineralogic phase-mapping software (V1.6.2). Prior to analysis, a thin film (approximately 25 nm thick) of electrically conductive carbon was applied to the polished surfaces using an AGAR Turbo Carbon Coater, evaporation-coating unit. Samples were examined under high vacuum conditions (10^{-4} Pa), at an accelerating voltage of 15 keV and a working distance of 10 mm.

SEM hosted EDX systems determine the energies of characteristic X-rays that are emitted where the electron beam interacts with the sample and can be used to identify elemental compositions and host phases. The EDX system used is capable of detecting elements from atomic numbers 4 (B) to 92 (U), and has detection limits of the order of 0.2–0.5 wt% for most common elements.

Digital photomicrographs were obtained using the backscatter electron (BSE) technique, recorded as 8-bit greyscale TIF format images using Zeiss' high definition backscatter detector (HDBSD). The brightness of a phase under BSE imaging is proportional to its mean atomic number.

Mineralogic phase maps were run with the SEM operating with a 120 μm aperture and 'beam boost' activated to give a nominal beam current of 10 nA. Mapping was performed over a grid of frames using BSE images and EDX data were captured in turn for each frame, with a beam step size of 7.5 μm and a dwell time of 10 ms. BSE images were captured at a 0.47 μm resolution, with a per pixel dwell time of 0.9 μs. Phase identifications were based on the per pixel normalised quantitative EDX data (using ZAF quantification protocols) passed through expert-user-defined compositional filters. Outputs were formed by combining data from multiple adjacent fields of view, mosaicked into phase map images with associated BSE images. Additional single frame X-ray elemental and phase maps were obtained under the same SEM operating conditions using the Bruker Esprit software at full resolution (i.e. the same as the accompanying BSE image), to resolve specific features of interest at higher spatial resolution.

4.3. LECO and coulometric analyses

TIC was calculated as the difference between the TC and TOC contents of a subset of the basaltic samples using a LECO CS225 elemental analyser (University of Aberdeen). TIC contents were assessed following prior treatment of powdered samples with mineral acid and TOC determined by CO_2-evolution following combustion under excess oxygen. Veracity of TC analyses was verified by analysis of certified reference materials (JGb-1 and LECO standards); the TC content of aliquots measured at the same time as the samples was within the range of the certified values. This analysis was unreplicated.

The TIC of one of the basaltic samples (Blue Ridge) was also determined using a CM5015 coulometer with an AutoMate autosampler at the SEAPORT Stable Isotope Laboratory (University of Southampton/National Oceanography Centre). The instrument has detection limits between 0.11 and 0.22 wt% $CaCO_3$. Data was collected on four aliquots and mean and standard deviation values calculated.

5. Results

5.1. Carbonate mineral standards

The TGA curves for the ~75 mg standard carbonate samples indicate differing decarbonation temperatures and weight losses (Fig. 2), commensurate with literature sources. In order of increasing decarbonation (inflexion) temperature, magnesite decomposes at ~642 °C (51.59% weight loss), calcite at ~805 °C (43.97% weight loss), dolomite at ~807 °C (46.20% total weight loss), strontianite at ~1071 °C (29.56% weight loss) and witherite at ~1245 °C (19.47% weight loss).

Mass spectrometer CO_2 evolution profiles present broad, generally asymmetric peaks with flat backgrounds and are compared in Fig. 2. The different carbonate species produce different peak CO_2 evolution temperatures, although these are generally similar for calcite and dolomite, reflecting their shared reaction (Table 1), except for the additional shoulder to the lower temperature side of the dolomite profile. For all the standard samples, the time lag measured between the TGA inflected registration of the decarbonation reaction and detection of CO_2 at the MS is very small (typically $<\pm1$ °C, maximum ±2 °C).

The TGA trace for the Eire calcite standard shows a single weight loss event (~500–900 °C, inflexion at 805 °C) of 43.97% (Fig. 2a), equivalent to a stoichiometric calcite content of 100%, corroborating the XRD and XRFS analyses (Table 1S (Supplementary Material)). A single, Gaussian-like CO_2 evolution peak with a similar inflexion temperature of 805 °C and a marked asymmetry to the low temperature side accompanies the weight loss (Fig. 2a).

The Malawian dolomite standard also shows a single weight loss of 46.03% between ~500 and 900 °C (inflexion at 807 °C, Fig. 2b) equivalent to a dolomite concentration of 96.4%. This composition concurs with XRD analysis that identified small quantities of calcite and quartz in the standard (Table 1S (Supplementary Material)). Both the dolomite MS CO_2 evolution and DTG (differential thermogravimetric) profiles show a similar single major peak (inflexion at ~805 °C) taken to represent the decomposition of the $CaCO_3$-component. Both profiles also show a noticeable, lower temperature shoulder at ~765 °C attributed to the initial dolomite decomposition reaction (Fig. 2b, Table 1).

In comparison to the calcite and dolomite samples, the Greek magnesite standard shows a lower temperature, major weight loss of 52.10% between ~200 and 800 °C (inflexion at 608 °C), equivalent to 99.8% magnesite. Again, this composition is consistent with the trace quantities of quartz and calcite identified in the standard by XRD analysis (Table 1S (Supplementary Material)). The weight loss is associated with a concomitant major peak on the MS CO_2 evolution profile (608 °C, Fig. 2c), again showing an asymmetry towards the lower temperature. A smaller weight loss between ~400 and 520 °C (inflexion at 503 °C) is clearly shown on the DTG and CO_2 evolution profiles (Fig. 2c) but its cause remains unknown.

The single TGA weight loss event of 29.64% for the strontianite standard sample (~700–1200 °C, inflexion at 1028 °C, not figured) is equivalent to a stoichiometric strontianite content of 99.4%, corroborating the XRD analysis (Table 1S (Supplementary Material)). The weight loss is again accompanied by a Gaussian-like CO_2 evolution peak from the MS with an identical inflexion temperature (1028 °C) and marked asymmetry to the low temperature side.

The witherite sample shows a single, high temperature TGA weight loss of 22.30% between 800 and 1300 °C (inflexion at 1196 °C, not figured), indicating that it is a pure sample, as also suggested by XRD analysis (Table 1S (Supplementary Material)). The MS output records a single CO_2 evolution (peak maximum at 1195 °C).

The measured MS profile CO_2 peak areas vary in proportion to the stoichiometric CO_2 content of each of the mineral standards i.e. witherite (22.30%), strontianite (29.81%), calcite (43.97%), dolomite (47.73%) and magnesite (52.20%). This means that the smallest measurable peak areas produce the lowest LDL for magnesite and the highest LDL for witherite.

Small quantities of calcite diluted with much greater quantities of inert corundum consistently produced measurable quantities of evolved CO_2, even at ~100 ppm calcite concentrations. Although, due to difficulties in producing homogeneous mixtures outlined above, this was the lowest concentration tested, these results suggest that the technique is capable of distinguishing and quantifying even smaller (<100 ppm)

concentrations. Such dilutions were not prepared for the other carbonates.

Strikingly, both the decarbonation temperatures and the mass spectrometric peak CO_2-evolution temperatures also vary depending on the quantity of carbonate mineral present (Fig. 3). Smykatz-Kloss (1974) noted similar behaviour when using DTA and produced differing gradient 'curves of sample amount dependence' = PA-curves, from the German, 'Proben-Abhängigkeit' for >1 mg sample. For a range of masses (<0.1–~75 mg), the peak MS CO_2-evolution temperatures for each carbonate standard vary dramatically: magnesite 501–608 °C, calcite 590–805 °C, dolomite 618–805 °C, strontianite 788–1057 °C and witherite 969–1224 °C. This obviously has a critical effect on the interpretation of sample CO_2-evolution profiles and particularly the identification of carbonate mineral species and their quantification using TGA-MS.

Example evolved CO_2 vs mass carbonate mineral calibration curves are shown for calcite, dolomite and magnesite (Fig. 1S (Supplementary Material)). These show excellent linear trends and correlation coefficients (>0.99). Replicate analyses indicate small standard deviations (e.g. calcite ±3% at ±3σ) and demonstrate the reproducibility of the technique. Generally, the lower the decarbonation temperature of the carbonate mineral, the greater the slope of the calibration curve. Magnesite therefore shows the greatest slope and witherite the shallowest slope for the analysed carbonate minerals. The following equations (3)–(6), also shown in Fig. 1S (Supplementary Material)) were used to determine the carbonate contents of the basaltic samples:

$$Integral\ CO_{2(calcite)}\ (nsA) = 223.45wt.\ calcite\ (mg) + 4.95 \quad (3)$$

$$Integral\ CO_{2(dolomite)}\ (nsA) = 276.35wt.\ dolomite\ (mg) + 0.21 \quad (4)$$

$$Integral\ CO_{2(magnesite)}\ (nsA) = 345.52wt.\ magnesite\ (mg) - 2.47 \quad (5)$$

$$Integral\ CO_{2(strontianite)}\ (nsA) = 178.63wt.\ strontianite\ (mg) + 1.78 \quad (6)$$

5.2. Basaltic samples

CO_2 evolution profiles for the ERW basaltic samples (Figs. 4 and 5) are more complex than those recorded for the individual carbonate mineral standards (Fig. 2). Relatively low temperature peaks (maxima at <100 and ~300–500 °C) were attributed to the decomposition/oxidation of small quantities of organic matter present in the basaltic samples. Oxidation of organic matter is possible as the flowing N_2 (99.998% pure) contains small quantities of O_2. Comparison of higher CO_2-evolution peak temperatures (>500 °C) with the evolution temperatures for the mineral standards were used to determine the nature and quantify the presence of any carbonate mineral(s) present (Table 3).

SEM analysis combined with Mineralogic microgeochemical mapping highlighted the complex mineralogy and grain inter-relationships of the basaltic samples (Figs. 6–9, 2S, 3S (Supplementary Material)). As anticipated from previous XRD analyses, the samples were composed of various proportions of plagioclase feldspar, pyroxene, quartz, K-feldspar, amphibole, Fe–Ti oxide, basaltic glass, apatite, chlorite, smectite, analcime and epidote (cf. Lewis et al., 2021). The microgeochemical mapping also successfully identified small quantities of various carbonate minerals in the basaltic materials.

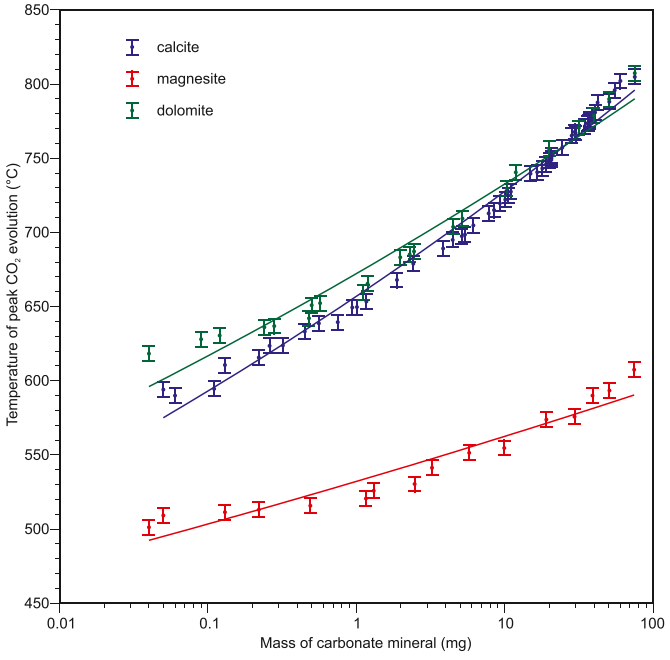

Fig. 3. Peak CO_2 evolution temperatures vs mass of carbonate standard.

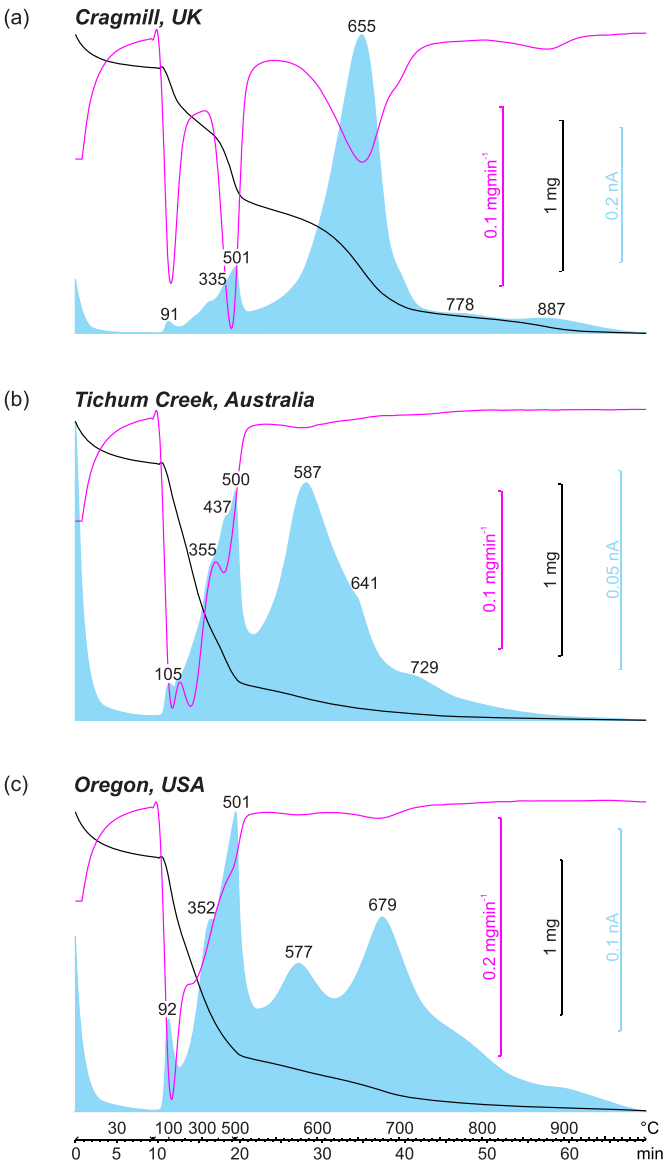

Fig. 4. TGA (black line), DTG (magenta line) and evolved CO_2 profiles (blue integrated area) for the ERW basaltic samples I. Numerical labels relate to peak maxima on the CO_2 evolution profiles. [Contains Data © University of Sheffield].

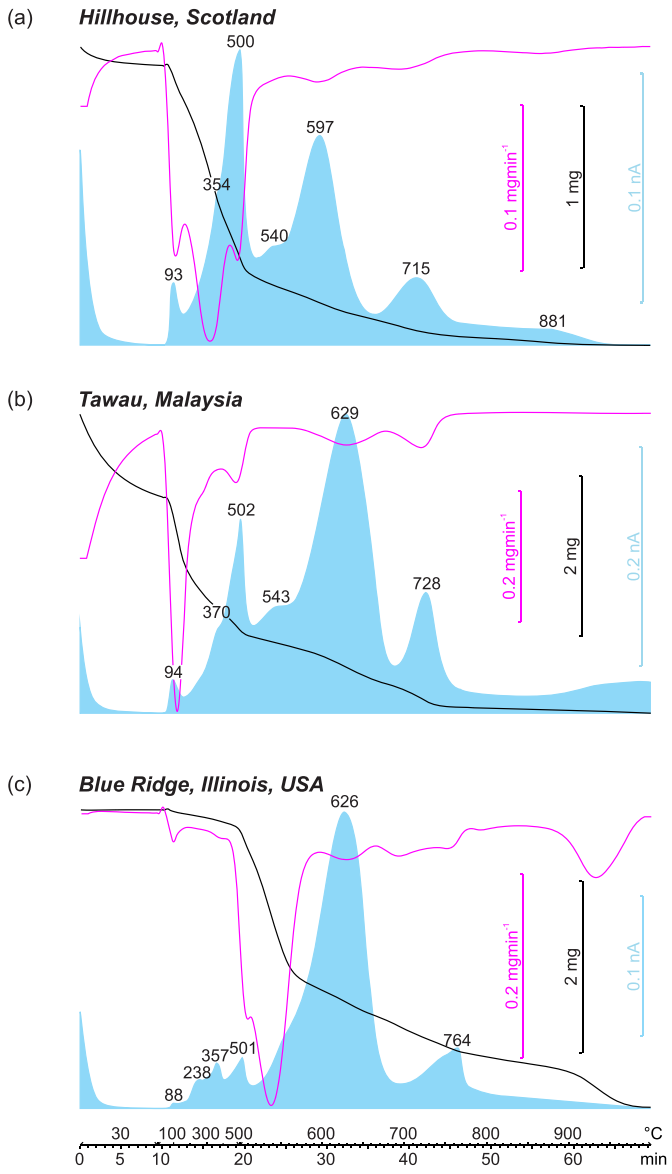

Fig. 5. TGA (black line), DTG (magenta line) and evolved CO_2 profiles (blue integrated area) for the ERW basaltic samples II. Numerical labels relate to peak maxima on the CO_2 evolution profiles. [Contains Data © University of Sheffield].

5.2.1. Cragmill, UK

The Cragmill material produces the simplest of the CO_2 evolution profiles for the basaltic samples (Table 3, Fig. 4a). Two minor events at 91 and 501 °C (and a small shoulder at 335 °C) were attributed to the oxidation of labile and more recalcitrant organic matter respectively. Applying the carbonate calibration curves and peak evolution temperatures, the intense CO_2 evolution at 655 °C is equivalent to 12528 ppm calcite, the largest carbonate-mineral content of the basaltic sample batch. A minor shoulder to the main CO_2 evolution peak was also detected (peak maximum at 778 °C) and was interpreted as representing the presence of 318 ppm strontianite. A broad, low intensity hump in the CO_2-evolution profile peaking at 887 °C could not be definitively ascribed to the decomposition of any particular carbonate mineral phase.

SEM analysis and Mineralogic mapping identified very rare, coarse-grained (>200 μm) rhombs of calcite that form ~0.8 wt% sample with even rarer fine-grained (<10 μm) fragments of dolomite (Fig. 6). No strontianite was detected by SEM/microgeochemical mapping.

5.2.2. Tichum Creek, Australia

Seven events were identified at ~105, 355, 437, 500, 587, 641 and 729 °C on the complex CO_2 evolution profile for the Australian basalt (Table 3, Fig. 4b). The four lower temperature events (~105, 355, 437 and 500 °C) were attributed to the decomposition/oxidation of organic matter. The DTG trace indicates three major events in this range at slightly different peak temperatures (~119, 232 and 434 °C), being augmented by the larger-scale evolution of H_2O (not shown), most likely also resulting from organic matter but potentially also clay mineral decomposition. The major CO_2 event at 587 °C, with a high temperature shoulder at 641 °C, was attributed to the presence of 1880 ppm calcite. A minor, higher temperature event at 729 °C was ascribed to the presence of 325 ppm strontianite, although this represents a lower peak evolution than the equivalent quantity of the strontianite standard. Triplicate analysis of the Australian basalt sample indicates an error of ±62 ppm (±3σ) for the calcite concentration.

SEM analysis/Mineralogic mapping of the Tichum sample again identified only rare, coarse-grained (>250 μm) crystals of calcite that form ~0.5 wt% material. The internal texture of the crystals suggest that they most likely represent fragments of fracture-fill mineralisation in the basalt (Fig. 7).

5.2.3. Oregon, USA

The Oregon basalt CO_2 evolution profile shows the most intense low temperature, organic matter oxidation peaks for the sample batch at 92, 352 and 501 °C (Table 3, Fig. 4c). The two carbonate mineral CO_2 peak evolutions at 679 and 577 °C represent equivalent calcite concentrations of 2845 and 2115 ppm respectively. However, these peak evolution temperatures appear higher and lower than those measured for equivalent masses of calcite standard.

SEM analysis/Mineralogic mapping identified rare crystals of calcite but these were exceptionally large (~800 μm) compared to the other basaltic samples (Fig. 2S (Supplementary Material)). This heterogeneity resulted in Mineralogic estimating the calcite concentration to be the highest for the sample batch at ~4.0 wt%. No other carbonate-bearing minerals were identified in this sample by SEM analysis or geochemical mapping.

5.2.4. Hillhouse, Ayrshire, Scotland

The CO_2 evolution profile for the Hillhouse basalt shows four major events at 93, 500, 597 and 715 °C together with less distinct events at 354, 540 and 881 °C (Table 3, Fig. 5a). The two, major low temperature

Table 3
Summary of >500 °C evolved CO_2 features and carbonate mineral attribution for the ERW basaltic samples. [Contains Data © University of Sheffield].

Locality	CO_2 evolution 1		CO_2 evolution 2		Comments
	Peak temp (°C)	Attributed to	Peak temp (°C)	Attributed to	
Cragmill, Northumberland, UK	655	12528 ppm calcite	778	318 ppm strontianite	–
Tichum Creek, Queensland, Australia	587	1880 ppm calcite	729	325 ppm strontianite	Shoulder at 641°C
Oregon, USA	679	2845 ppm calcite	577	2115 ppm calcite	–
Hillhouse, Troon, UK	597	2374 ppm calcite	715	614 ppm strontianite	Shoulder at 540 °C
Tawau, Sabah, Malaysia	629	8497 ppm calcite	728	1069 ppm strontianite	Shoulder at 543°C
Blue Ridge, Illinois, USA	626	6706 ppm calcite	764	481 ppm strontianite	–

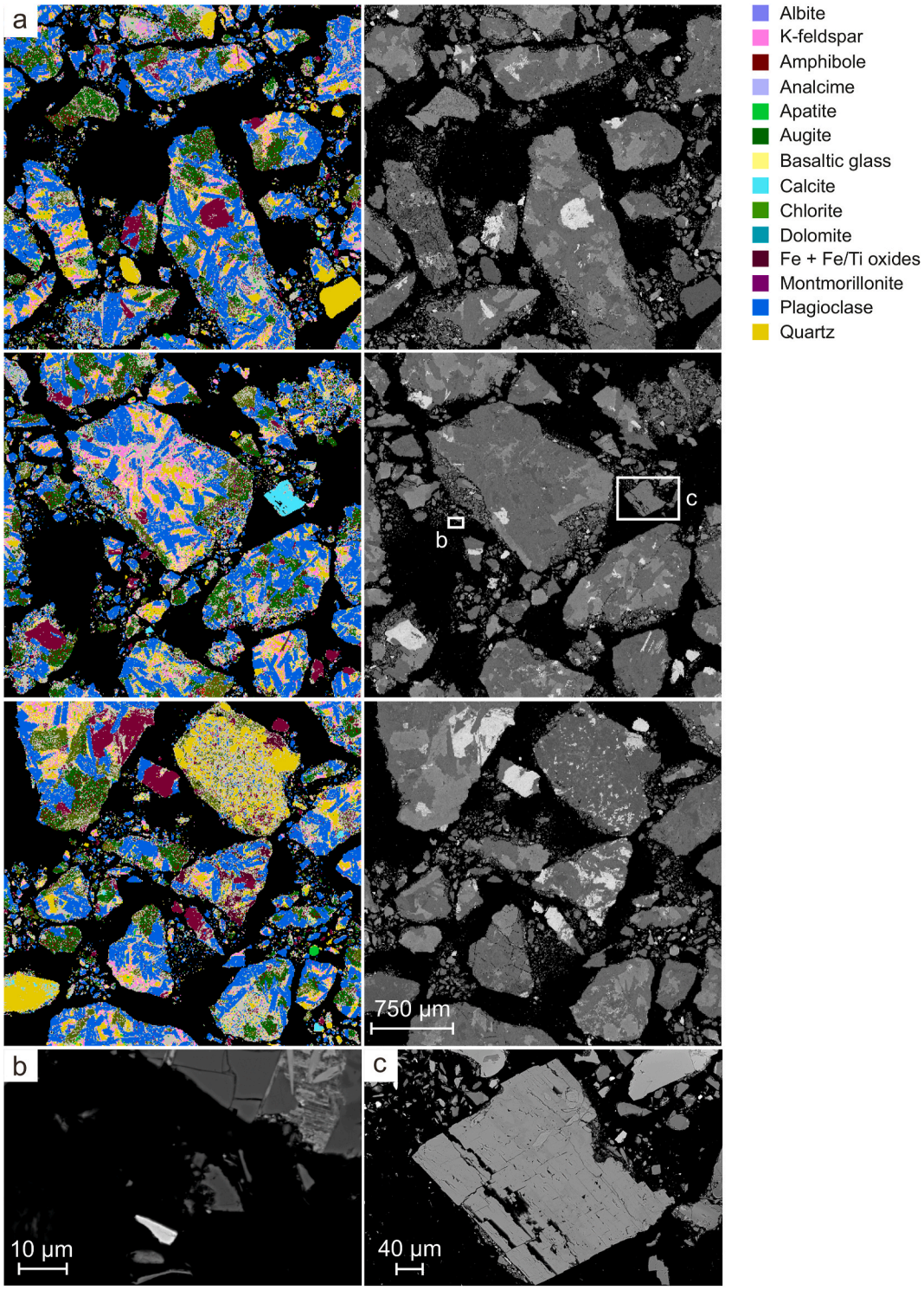

Fig. 6. Cragmill sample. a. Montage of Mineralogic microgeochemical mapping images (coloured, left) and equivalent backscattered scanning electron photomicrographs (monochrome, right) for three selected areas. Inset boxes indicate areas shown in higher magnification in b. and c. b. Backscattered scanning electron photomicrograph of very rare, fine-grained (<10 μm) irregular, angular dolomite fragment (right of centre, intermediate brightness, no growth zoning visible). c. Backscattered scanning electron photomicrograph of rare, coarse-grained (>200 μm) calcite rhomb. The variation in backscatter brightness reflects variations in Fe and Mn content.[Contains Data © University of Sheffield].

features (93 and 500 °C) are relatively sharp and were attributed to the oxidation of organic matter. The 597 °C event represents the greatest mass of evolved CO_2, equivalent to 2374 ppm calcite. A subordinate event at 715 °C was ascribed to the decomposition of 614 ppm strontianite. Again, the TGA and DTG curves show an additional weight loss, peaking at ~320 °C, which was attributed to the dehydroxylation of clay minerals in the altered basalt and evidenced on the MS H_2O evolution profile (not shown). A small shoulder at 540 °C on the CO_2 evolution profile could not be definitively explained.

SEM analysis/Mineralogic mapping suggest that the Hillhouse basalt contains small quantities of calcite (~0.1 wt%) together with elongate Fe-dolomite crystals (~0.04 wt%) with Fe-rich inclusions (Fig. 8).

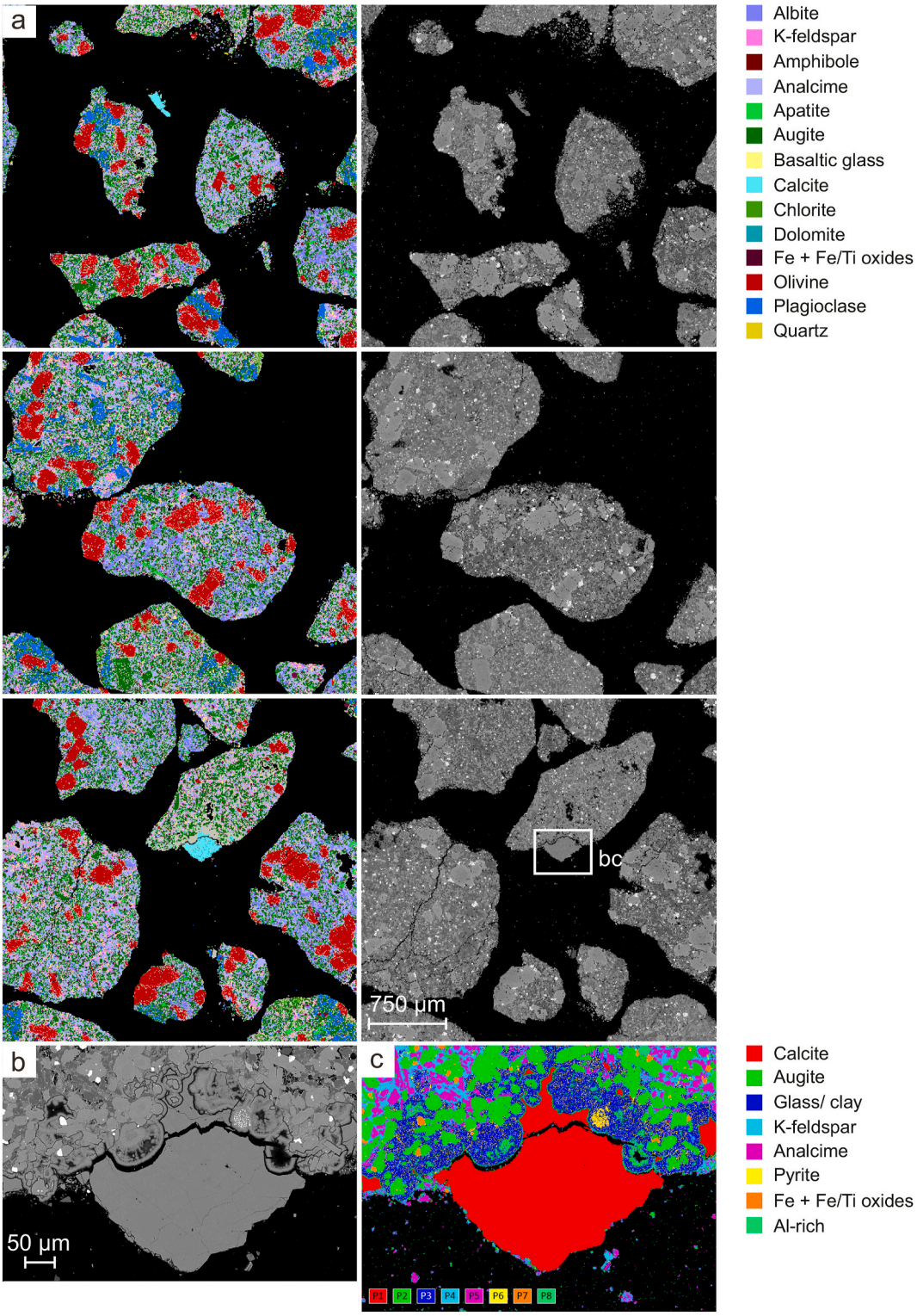

Fig. 7. Tichum Creek, Australia sample. a. Montage of Mineralogic microgeochemical mapping images (coloured, left) and equivalent backscattered scanning electron photomicrographs (monochrome, right) for three selected areas. Inset boxes indicate areas shown in higher magnification in b. and c. b. Backscattered scanning electron photomicrograph of rare, coarse-grained (>250 μm) crystals of calcite. The internal texture of the crystals suggest that they are *in situ* and most likely represent fragments of fracture-fill mineralisation in the basalt. The calcite in this sample is notable for typically containing >2 wt% Mg. c. Coloured PhaseMap of equivalent area to b. [Contains Data © University of Sheffield].

5.2.5. *Tawau, Malaysia*

The features of the CO_2 evolution profile for the Malaysian basalt (Table 3, Fig. 5b) are similar to those observed for the Hillhouse basalt. Although less intense, the organic matter oxidation features have maxima at very similar temperatures (major features at 94 and 502 °C, minor feature at 370 °C). The most intense evolution at 629 °C, represents an equivalent calcite concentration of 8497 ppm. The smaller event at 728 °C was attributed to the decarbonation of 1069 ppm

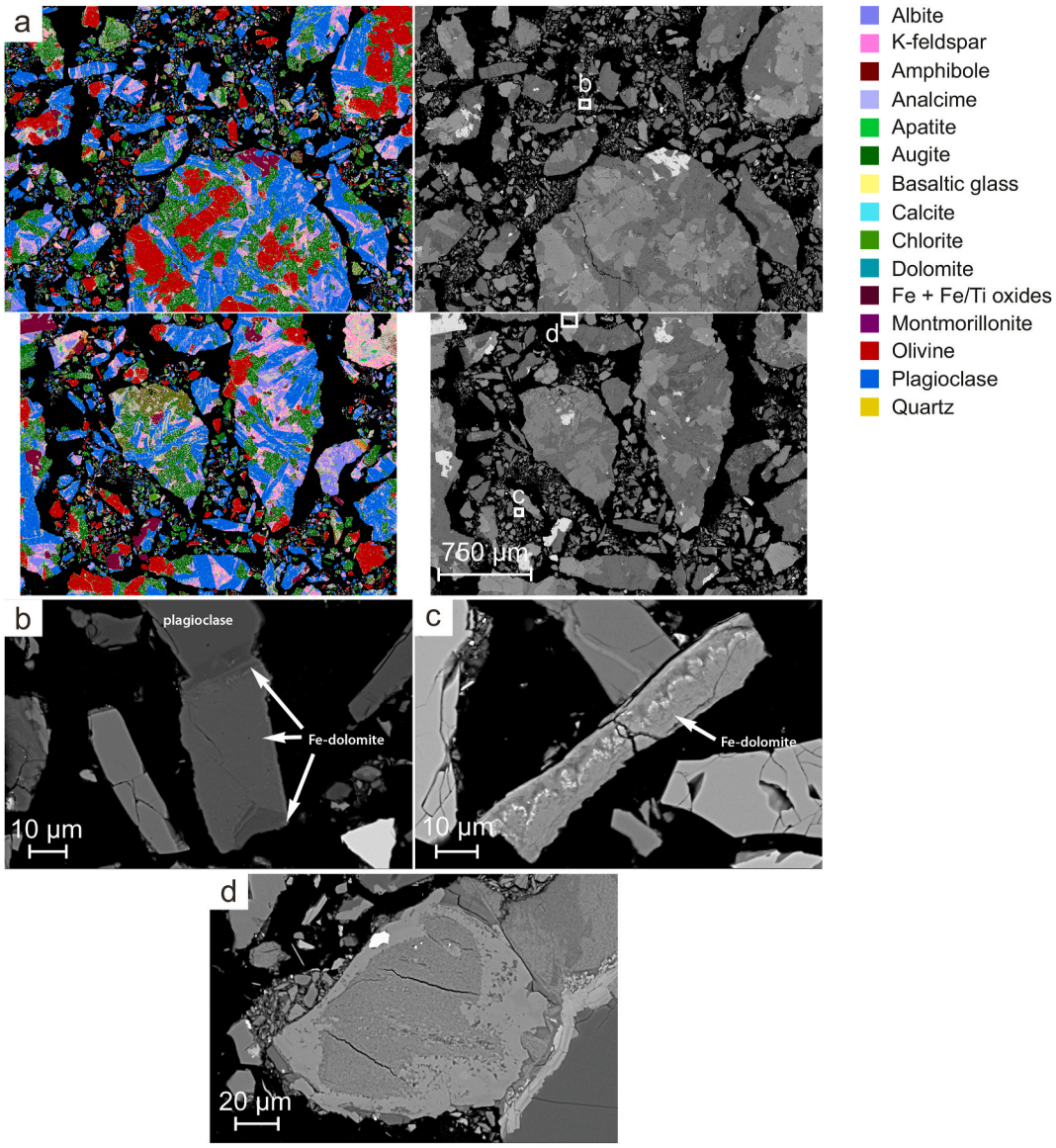

Fig. 8. Hillhouse, Troon sample. a. Montage of Mineralogic microgeochemical mapping images (coloured, left) and equivalent backscattered scanning electron photomicrographs (monochrome, right) for three selected areas. b. Backscattered scanning electron photomicrograph of Fe-dolomite and plagioclase crystals. c. Backscattered scanning electron photomicrograph of elongate Fe-dolomite crystals with Fe-rich inclusions (shown bright). d. Backscattered scanning electron photomicrograph of a rare calcite-bearing particle. The calcite has formed by encircling chlorite (centre), possibly replacively. The chlorite itself has formed through alteration of pyroxene, remnants of which are also enclosed by the calcite (right of top). [Contains Data © University of Sheffield].

strontianite. No conclusive explanation could be found for the shoulder in the CO_2 profile at 543 °C, other than it is very similar to that shown by the Hillhouse basalt.

Only very rare calcite crystals (~0.1 wt%) were identified by SEM analysis and Mineralogic mapping (Fig. 3S (Supplementary Material)).

5.2.6. Blue Ridge, Illinois, USA

Triplicate CO_2 evolution profiles for the Illinois basalt shows similar features to the Malaysian and Hillhouse samples (Table 3, Fig. 5c). Minor, low temperature maxima at 501, 357 and 88 °C with a shoulder at 238 °C were taken to represent the oxidation of organic matter. The major feature of the profile has a maximum at 626 °C and was therefore ascribed to calcite decarbonation, representing an average concentration of 6706 ± 430 ppm (±3σ). A minor feature at 764 °C represents the presence of 481 ± 43 ppm (±3σ) strontianite in this basalt.

SEM analysis/Mineralogic mapping identified small quantities of calcite in this basalt (~0.9 wt%). The calcite predominantly occurs as a replacive cement (<40 μm) but also rarely as larger, discrete crystals (~150 μm) (Fig. 9).

5.2.7. TIC, TOC analyses

LECO data also indicates the presence of low levels of total organic carbon (TOC, Table 2) in the basalt samples (0.013–0.020 wt%) which appear to be similar to those indicated by the low temperature CO_2-evolutions shown by TGA-MS. Total inorganic carbon (TIC) values (0.019–0.411 wt%, Table 2) from LECO analysis suggest equivalent calcite contents in the range 0.16–3.42 wt%, generally greater than the proportions predicted by TGA-MS. Coulometric analysis of the Blue Ridge basalt suggests a carbonate (calcite) content of 0.68 ± 0.12 wt%, based on four aliquots.

6. Discussion

6.1. Detection and quantification

Since straight-line calibration curves were generated for the evolved

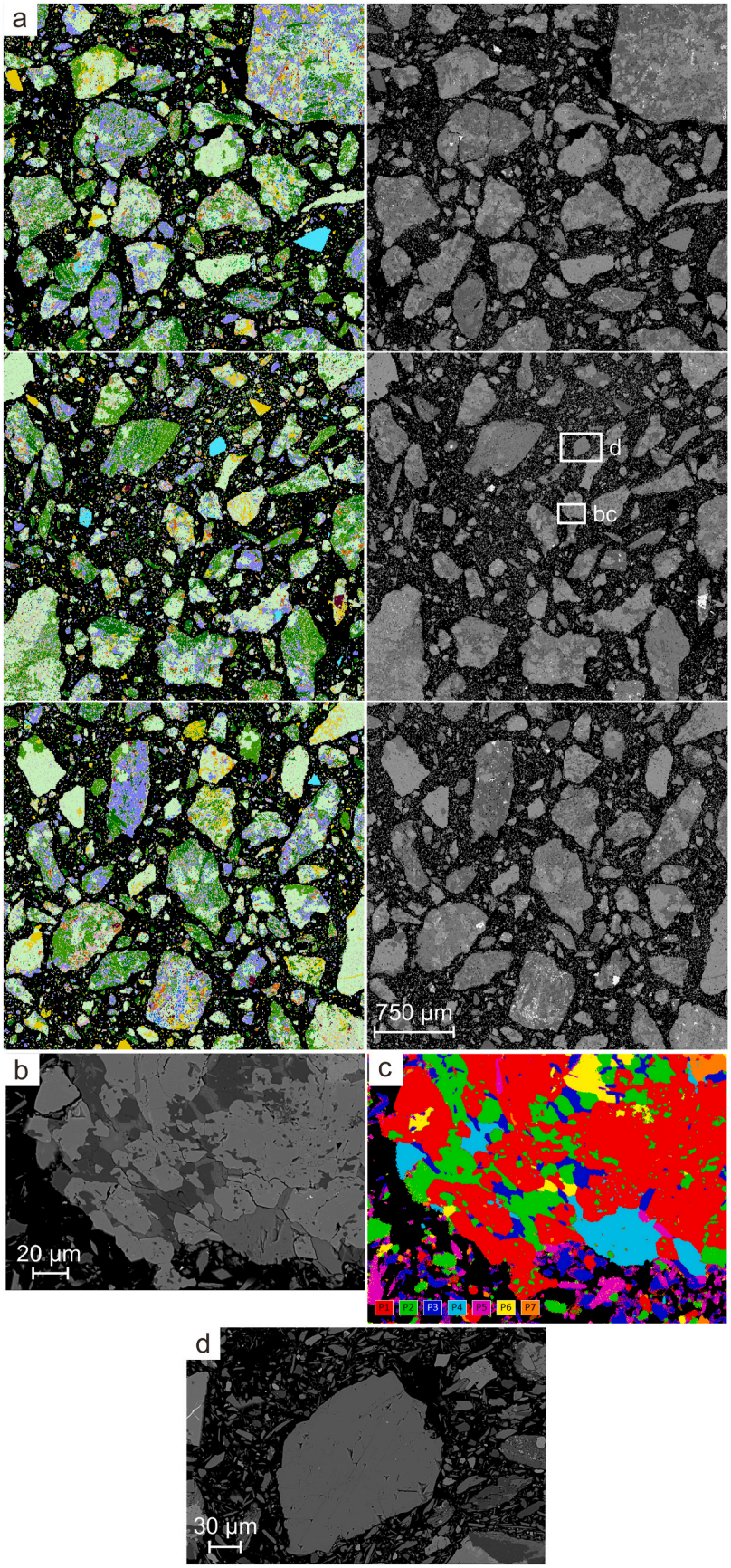

Fig. 9. Blue Ridge, Illinois sample. a. Montage of Mineralogic micro-geochemical mapping images (coloured, left) and equivalent backscattered scanning electron photomicrographs (monochrome, right) for three selected areas. Inset boxes indicate areas shown in higher magnification in b., c. and d. b. Backscattered scanning electron photomicrograph of replacive calcite cement (<40 µm). c. Coloured PhaseMap of equivalent area to b. d. Backscattered scanning electron photomicrograph of rare, larger, discrete calcite crystal (~150 µm). [Contains Data © University of Sheffield].

CO_2 ($R^2 > 0.99$), the lowest limit of detection is determined by the ability to measure a peak area. In practice, the smallest measurable peak area is the smallest one that can be unambiguously distinguished from baseline noise and is described in terms of the signal to noise ratio (S/N). ACS guidelines suggest that a S/N = 10 defines the smallest peak whose area can be measured with acceptable precision for quantification purposes (MacDougall and Crummett, 1980).

SEM microanalysis of polished block mounts has corroborated the presence of the different carbonate minerals (calcite and dolomite) in the ERW basaltic samples, but we have demonstrated that the TGA-MS is capable of detecting much lower (~100 ppm) concentrations. Although not proven, it is likely that the technique is capable of detecting even lower (<100 ppm) carbonate mineral concentrations. A consistent, high temperature TGA-MS CO_2 evolution has here been attributed to the decomposition of strontianite, which is feasible for basaltic lithologies. A close overlap of the silicon K-alpha and strontium L-alpha X-ray lines makes identification of strontium-bearing mineral phases in a silicate-rich rock very challenging when using SEM-EDX techniques. This is particularly so for the short beam dwell times used in the large area mineral phase mapping protocol applied here. These factors together with the suggested low (318–1069 ppm) concentrations, most likely explain why strontianite was not detected by SEM microanalysis.

The generated CO_2 evolution profiles for the ERW basaltic samples have been attributed to a range of different organic compounds and carbonate minerals at different concentrations.

6.2. Organic matter decomposition

The slow thermal oxidation of soil organic matter in flowing air/oxygen gas streams has been well characterised as labile organic matter ('cellulose', 200–380 °C), recalcitrant organic matter ('lignin', 380–475 °C) and refractory organic matter (475–650 °C) including black carbon (e.g. Lopez-Capel et al., 2005). However, organic matter thermal decomposition in a N_2 atmosphere is less well understood and can be difficult to interpret due to the complexity of a range of fusion, decomposition and polymerization reactions (Guo et al., 2016). Nevertheless, Boguta et al. (2017) distinguished approximately similar temperature ranges (volatile and labile groups, 220–430 °C and recalcitrant and refractory structures, 430–650 °C) for soil-derived natural polymers, fluvic and humic acids. Further data has been produced by thermal instrumentation on the Phoenix and MSL spacecraft employing inert (N_2 or He) carrier gas (e.g. Archer et al., 2013; Sutter et al., 2017). Here, the authors ascribed CO_2 evolution to organic compound decomposition including the combustion of simple organic carbon (<350 °C), refractory macromolecular carbon (300–600 °C) or the decarboxylation of organic compounds (carboxylic acids, oxalates etc, 150–800 °C) (Mu and Perlmutter, 1981; Sutter et al., 2017).

Based on similar CO_2 evolution temperatures, small quantities of organic matter have been detected in all of the ERW basaltic samples in this study. Since fresh basalt does not contain organic matter, it is most likely that the detected organic matter represents contamination with soil or anthropogenic materials.

6.3. Carbonate mineral decarbonation

Although it is acknowledged that a small proportion may be due to the higher-temperature decomposition of organic matter, the >500 °C CO_2 evolution from the ERW basaltic samples is here attributed to the decarbonation of carbonate minerals.

Despite their differing geographic locations, basalt types, mineral compositions and subsequent alteration histories, TGA-MS analyses suggest that the basaltic materials examined in this study all contain small quantities of various carbonate minerals.

The Cragmill basalt has the greatest concentration of carbonate-mineral (12528 ppm calcite and 318 ppm strontianite). Full mineralogical analysis (Lewis et al., 2021) indicates that, although this sample is predominantly composed of feldspar (plagioclase and K-feldspar) as would be expected of a basalt, it also contains appreciable clay minerals (~10% chlorite-smectite) and ~7% quartz. The presence of significant carbonate minerals together with clay minerals and quartz suggest that this basalt has undergone hydrothermal alteration following initial crystallisation (e.g. Seyfried and Bischoff, 1974). Brief SEM examination also identified coarse-grained rhombic crystals of calcite, most likely to have formed from hydrothermal fluid interaction and precipitated as fracture-fill. As for all the quarried basalt samples, contamination of the Cragmill basalt with other rock fragments (e.g. limestone) represents a further potential source of carbonate minerals in these materials.

The greater concentrations of quartz (~19%) together with clay minerals (saponite) identified in the Tawau basalt (Lewis et al., 2021) suggests that it has undergone a greater degree of hydrothermal alteration/weathering but this has not resulted in a similar scale of carbonate mineral precipitation (8497 ppm calcite and 1069 ppm strontianite).

Even smaller quantities of calcite were identified in the other basalts; in descending concentration: Blue Ridge (6706 ppm), Oregon (2845 ppm), Hillhouse (2374 ppm) and Tichum Creek (1880 ppm). SEM observation of replacive calcite cement (<40 μm) and rare larger, discrete grains together with full mineralogical analyses (Lewis et al., 2021) again suggest that hydrothermal alteration/weathering was responsible for the precipitation of carbonates in these basalts, but that these processes were less advanced than for the Cragmill and Tawau basalts.

The co-incidence of the peak CO_2 evolution for calcite and dolomite (Fig. 2), with the exception of the shoulder at ~765 °C recorded for dolomite, means that the small quantities of calcite identified in the basalts could equally wholly or partially be ascribed to dolomite. Comparison of the temperatures of peak CO_2 evolution for the basalt samples with those obtained from carbonate mineral standards (Fig. 3) confirm that these should be ascribed to calcite with the possible exception of the Oregon basalt where a higher evolution temperature (679 °C) would appear closer to dolomite.

SEM analysis identified possible trace quantities of Fe-dolomite in only one of the samples (Hillhouse) and failed to detect ankerite or siderite in any of the samples. Consequently, the CO_2-evolution profiles of the solid-solution series Fe-dolomite, ankerite and siderite have not been considered as part of this study. Previous studies indicate that siderite decarbonates between 500 and 550 °C and both ankerite and Fe-dolomite dissociate via three reaction steps between 700 and 950 °C (e.g., Milodowski and Morgan, 1980; Földvári, 2011). However, decomposition temperatures are dependent on the species chemistry and the nature of Fe^{2+}, Mg^{2+} and Mn^{2+} substitution. For these reasons, further work would be required to discriminate subordinate amounts of these species in the presence of other carbonates.

Strontianite is a rarely-described component of basalts (e.g., Meixner, 1964), most likely reflecting its low–very low concentration. However, as the average Sr concentration of basalts is ~400 ppm (Gale et al., 2013), coupled with the very recent discovery of celestine ($SrSO_4$) in moderately altered recent oceanic Hawaiian basalts (Garcia and Hellebrand, 2020), the quantities of strontianite suggested by TGA-MS analysis appear plausible. Strontium, along with Eu and to a lesser extent Ba, can substitute for Ca in plagioclase feldspar. Hydrothermal experiments have observed the liberation of Sr to solution during albitization reactions (e.g. Hövelmann et al., 2010). A low temperature (<100 °C) hydrothermal vein-fill development would appear most likely for strontianite.

This study has demonstrated that mass spectrometric peak CO_2 evolution temperature is related to the mass of carbonate mineral present, with large ranges in peak evolution temperatures measured for different carbonate species e.g. magnesite 501–613 °C, calcite 583–813 °C, dolomite 618–808 °C, strontianite 788–1057 °C and witherite 969–1224 °C. Smykatz-Kloss (1974) previously published similar PA curves for DTA of >1 mg mineral but did not offer any reason for the noted behaviour. Most likely this phenomenon reflects reaction

kinetics, whereby if more carbonate mineral is present, the time taken for complete decarbonation is extended, increasing the peak evolution- and weight loss-temperatures. Such peak evolution temperature ranges certainly complicate the interpretation of CO_2-profiles, but the present study provides a basis for more precise identification and quantification. The range in peak evolution temperature also explains why the trace quantities of calcite identified by XRD in both the dolomite and magnesite standards, did not produce discriminatory CO_2 evolution peaks, as these were 'hidden' beneath the more substantial evolution of the dominant carbonate species.

6.4. TGA-MS of carbonates in other basaltic materials

Small amounts of carbonate-group minerals have often previously been described in basalts, most usually as vesicle- or cavity-fillings (e.g. Lavoie, 1995; Otterns et al., 2019), hydrothermal veins (Brandstätter et al., 2018; Hernández-Uribe et al., 2020) or as weathering/alteration products replacing phenocrysts (e.g. Churchman and Lowe, 2012; MacDonald et al., 2019). However, these have rarely been quantified; and certainly not at the low levels discussed in this study.

Calcite is also a common reaction product in basalt carbonation studies, for example *in situ* mineralisation where supercritical CO_2 is injected into basalt formations (McGrail et al., 2006; Pogge von Strandmann et al., 2019) or reacted in laboratory experiments (e.g. Schaef et al., 2009; Kumar and Shrivastava, 2019). Modelling of the reaction of basalt with carbonated water suggests that dolomite and magnesite are amongst the precipitates formed after ~1 year, with substantially greater mineralisation after 10–100 years (Marini, 2007). Batch experiments produce magnesite from olivine dissolution at faster timescales (e.g. Rosenbauer et al., 2012; Sissmann et al., 2014).

The detection and quantification of carbonate minerals in 'starting' and 'end-product' materials is therefore clearly important to ongoing modelling and experimental studies (e.g. Lewis et al., 2021).

Interestingly, NASA has deployed similar technology to analyse rocks and soils on its robotic missions to Mars since 2008. The 1976 Viking 1 and 2 spacecraft first carried gas chromatograph-MS systems but failed to detect organic compounds in the Martian soil (Fenselau et al., 2003).

The later Phoenix Lander's Thermal and Evolved Gas Analyser (TEGA), consisting of a calorimeter coupled to an MS, first detected a high-temperature endotherm (~725–820 °C) and associated CO_2 evolution which was assigned to either calcite or aragonite in the Wicked Witch soil (Boynton et al., 2009). A lower temperature (~400–680 °C) CO_2 evolution was tentatively apportioned to some combination of Mg-carbonate, Fe-carbonate, adsorbed CO_2 from a zeolite-like phase and/or organic molecules converted to CO_2 by soil oxidants (Boynton et al., 2009). Later, low-pressure experiments (more accurately simulating the Mars atmosphere) suggested that the high temperature endotherm might represent calcite, ankerite, dolomite or a calcium-rich carbonate with Fe and/or Mg solid solution chemistry. Siderite and magnesite were candidates for the lower-temperature CO_2 release (Sutter et al., 2012).

The Curiosity rover exploration of Gale crater (2012–present) carried the Sample Analysis at Mars (SAM) instrument including an MS to analyse evolved gases (including CO_2) from basaltic sediments and bedrock samples following heating to ~870 °C (Sutter et al., 2017). The samples were typically composed of feldspar, pyroxene, olivine, iron oxides and clay minerals, similar to weathered basaltic soils on Earth. CO_2 was detected over most of the temperature interval and attributed to atmospherically adsorbed CO_2, organic carbon, CO_2 inclusions in mineral/glass phases and carbonate minerals. Most CO_2 was evolved below 450 °C, consistent with derivation from organic material. Evolved CO_2 between 450 and 800 °C was attributed to low concentrations (<0.7 ± 0.1 wt%) of various different carbonate minerals (Fe-rich, Mg-rich and Fe–Mg carbonate) that were undetected by Curiosity's CheMin (XRF/XRD) instrumentation (Sutter et al., 2017).

6.5. TGA-MS compared to other methods

The calculated TGA-MS carbonate mineral concentrations are lower, sometimes substantially lower than those derived from LECO TIC measurements for the Oregon, Malaysian and Blue Ridge basalts (Tables 2 and 3). Exceptionally the Cragmill sample has a higher TGA-MS carbonate mineral content compared to the LECO TIC determination, but although these two samples were taken from the same quarry, they are actually different samples. For example, TGA-MS suggests that the Blue Ridge basalt contains 0.54% calcite while LECO TIC determinations indicated an equivalent 3.43% calcite.

Literature sources suggest that LECO TOC measurements for geological samples provide results within ±5% value at the 95% confidence limit (e.g. Mahoney et al., 2019). However, since LECO TIC determinations are produced from the difference between TC and TOC determinations, accurate TIC values are therefore reliant on both accurate TC and accurate TOC determinations. As noted by Weliky et al. (1983), the issue with such LECO analyses lies not with the conversion of TC to CO_2 or the detection of CO_2 evolved, but with the techniques used to partition TC between OM and carbonate minerals. Organic C can be removed by burning at 500 °C for 2 h or carbonate minerals can be removed with acid but neither technique is sufficiently selective as to not affect the carbon in the remaining phase. As we have demonstrated, some carbonate minerals may begin to decarbonate at or below 500 °C, negating differentiation between organic and inorganic carbon on a decomposition temperature basis. Acid removal of mineral carbonates is also unsatisfactory since firstly, different carbonate species have different dissolution reaction rates (e.g. Peng et al., 2016) and secondly some organic carbon may also be removed (Froelich, 1980). The dependence of the measured quantity of each carbon phase on the other, using either technique, can lead to multiple and compounding errors and misleading correlations between TIC and TOC (Weliky et al., 1983).

Low TOC values (causing major errors in TIC) have previously been recognised, particularly where samples are not homogenised (Raja and Barron, 2020), where drying or pre-treatment to remove carbonates may result in the loss of volatile organic compounds or the decomposition and loss of other organic compounds (Schumacher, 2002) or where refractory 'cokes' are present and incomplete decarbonisation occurs (Liu et al., 2019). High TOC values can be produced if carbonate or sulphur-bearing compounds or water have not been removed prior to LECO analysis.

If the TIC value obtained from coulometric analysis of the Blue Ridge basalt is wholly attributed to calcite (0.68 ± 0.12 wt%), this represents a very similar value and again corroborates the concentration obtained by TGA-MS (0.67 wt%).

TGA-MS data, corroborated by SEM/Mineralogic mapping and coulometric analysis, suggests that TGA-MS offers a more precise technique than LECO for the quantification of carbonate species, particularly at low levels. Unlike coulometric analysis, TGA-MS also uniquely offers the ability to speciate the nature of the carbonate species present.

7. Conclusion

This study has confirmed that coupled TGA-MS analysis provides a relatively rapid, effective technique for the detection and quantification of carbonate mineral species in ERW basaltic materials. Analysis only requires small (<75 mg) sample mass and is therefore ideal for homogenised laboratory experimental residues and field demonstrator samples.

As corroborated by SEM-EDS mapping, TGA weight losses can provide accurate information on carbonate mineral speciation and quantification. However, MS-detected CO_2 evolution provides such data at even lower concentrations with a proven LDL of ~100 ppm for calcite. It is likely that the technique can detect even lower (<100 ppm) concentrations of carbonate minerals.

TGA-MS analyses have determined small (<12528 ppm) but

consistent carbonate contents in six different basaltic materials from widely different geological and geographical settings, employed as ERW materials. Such information is an important input for reactive transport modelling to critically assess ERW and the efficacy of different potential basalt resources.

As demonstrated on analogous basaltic rock and soil materials from Mars, TGA-MS provides a very useful technique for an even wider range of research.

Funding

ALL's input to this study was supported by a NERC ACCE DTP studentship. Otherwise, this research did not receive any specific grant from funding agencies in the public, commercial, or not-for-profit sectors.

Declaration of competing interest

The authors declare that they have no known competing financial interests or personal relationships that could have appeared to influence the work reported in this paper.

Data availability

Data will be made available on request.

Acknowledgements

The authors gratefully appreciate the support, advice and assistance of David Beerling and members of the Leverhulme Centre for Climate Change Mitigation, University of Sheffield. John Fletcher (BGS) is acknowledged for the skilled preparation of the polished, resin-impregnated blocks. Rachael James and Christopher Pearce (University of Southampton) are thanked for permission to use the LECO and coulometry analyses. Henry Holbrook (BGS) is thanked for drafting the graphical abstract. The authors are grateful to Alicja Lacinska, Benjamin Tutolo and an anonymous reviewer for their comments which considerably improved the manuscript. SJK and JCR publish with the permission of the Director, British Geological Survey (UKRI).

Appendix A. Supplementary data

Supplementary data to this article can be found online at https://doi.org/10.1016/j.apgeochem.2022.105465.

References

Allen, C.C., Gooding, J.L., Jercinovic, M., Kiel, K., 1981. Altered basaltic glass: a terrestrial analog to the soil on Mars. Icarus 45, 347–369. https://doi.org/10.1016/0019-1035(81)90040-3.

Alt, J.C., Honnorez, J., 1984. Alteration of the upper oceanic crust, DSDP site 417: mineralogy and chemistry. Contrib. Mineral. Petrol. 87, 149–169. https://doi.org/10.1007/BF00376221.

Archer, P.D., Ming, D.W., Sutter, B., 2013. The effects of instrument parameters and sample properties on thermal decomposition: interpreting thermal analysis data from Mars. Planetary Science 2, 2. https://doi.org/10.1186/2191-2521-2-2.

Bach, L.T., Gill, S.J., Rickaby, R.E.M., Gore, S., Renforth, P., 2019. CO_2 removal with enhanced weathering and ocean alkalinity enhancement: potential risks and co-benefits for marine pelagic ecosystems. Front. Climate 1, 7pp. https://doi.org/10.3389/fclim.2019.00007.

Beerling, D.J., 2017. Enhanced rock weathering: biological climate change mitigation with co-benefits for food security? Biol. Lett. 13, 20170149 https://doi.org/10.1098/rsbl.2017.0149.

Beerling, D.J., Leake, J.R., Long, S.P., Scholes, J.D., Ton, J., Nelson, P.N., Bird, M., Kantzas, E., Taylor, L.L., Sarkar, B., Kelland, M., DeLucia, E., Kantola, I., Müller, C., Rau, G., Hansen, J., 2018. Farming with crops and rocks to address global climate, food and soil security. Nature Plants 4, 138–147. https://doi.org/10.1038/s41477-018-0108-y.

Blanc-Betes, E., Kantola, I.B., Gomez-Casanovas, N., Hartman, M.D., Parton, W.J., Lewis, A.L., Beerling, D.J., DeLucia, E.H., 2021. In silico assessment of the potential of basalt amendments to reduce N_2O emissions from bioenergy crops. GCB Bioenergy 13, 224–241. https://doi.org/10.1111/gcbb.12757.

Boguta, P., Sokolowska, Z., Skic, K., 2017. Use of thermal analysis coupled with differential scanning calorimetry, quadrupole mass spectrometry and infrared spectroscopy (TG-DSC-QMS-FTIR) to monitor chemical properties and thermal stability of fulvic and humic acids. PLoS One 12 (12). https://doi.org/10.1371/journal.pone.0189653.

Boynton, R.S., 1980. Chemistry and Technology of Lime and Limestone, second ed. Wiley-Interscience, New York.

Boynton, W.V., Ming, D.W., Kounaves, S.P., Young, S.M.M., Ardvison, R.E., Hecht, M.H., Hoffman, J., Niles, P.B., Hamara, D.K., Morris, R.V., 2009. Evidence for calcium carbonate at the Mars Phoenix landing site. Science 325, 61–64. https://doi.org/10.1126/science.1172768.

Brandstätter, J., Kurz, W., Richoz, S., Cooper, M.J., Teagle, D.A.H., 2018. The origin of carbonate veins within the sedimentary cover and igneous rocks of the Cocos Ridge: results from IODP hole U1414A. G-cubed 19, 3721–3738. https://doi.org/10.1029/2018GC007729.

Capo, R.C., Whipkey, C.E., Blachère, J.R., Chadwick, O.A., 2000. Pedogenic origin of dolomite in a basaltic weathering profile, Kohala peninsula, Hawaii. Geology 28, 271–274. https://doi.org/10.1130/0091-7613(2000)28<271:PODIA>2.0.CO;2.

Charsley, E.L., Manning, N.J., Warrington, S.B., 1987. A new integrated system for simultaneous TG-DTA-MASS spectrometry. Thermochim. Acta 114, 47–52. https://doi.org/10.1016/0040-6031(87)80239-3.

Churchman, G.J., Lowe, D.J., 2012. Alteration, formation, and occurrence of minerals in soils. In: Huang, P.M., Li, Y., Sumner, M.E. (Eds.), Handbook of Soil Science. Properties and Processes, second ed. CRC Press, Taylor & Francis, Boca Raton, p. 172.

Cooper, H.V., Sjögersten, S., Lark, R.M., Girkin, N.T., Vane, C.H., Calonego, J.C., Mooney, S.J., 2021. Long-term zero-tillage enhances the protection of soil carbon in tropical agriculture. Eur. J. Soil Sci. 72, 2477–2492. https://doi.org/10.1111/ejss.13111.

Dallas, G., 2006. Taking Thermogravimetric Analysis to a New Level of Performance and Convenience. American Laboratory, p. TP015.

Edwards, D.P., Li, F., James, R.H., Pearce, C.R., Scholes, J., Freckleton, R.P., Beerling, D. J., 2017. Climate change mitigation: potential benefits and pitfalls of enhanced rock weathering in tropical agriculture. Biol. Lett. 13, 20160715 https://doi.org/10.1098/rsbl.2016.0715.

Engler, P., Santana, M.W., Mittleman, M., Balazs, D., 1989. Non isothermal in situ XRD analysis of dolomite decomposition. Thermochim. Acta 140, 67–76. https://doi.org/10.1016/0040-6031(89)87285-5.

Faust, G.T., 1950. Thermal analysis studies on carbonates, I-aragonite and calcite. Am. Mineral. 35, 207–224.

Fenselau, C., et al., 2003. Mass spectrometry in the exploration of Mars. J. Mass Spectrom. 38, 1–10. https://doi.org/10.1002/JMS.396.

Földvári, M., 2011. Handbook of thermogravimetric system of minerals and its use in geological practice. Occasional Papers Geol. Institute Hungary 213, 180. https://doi.org/10.1556/CEuGeol.56.2013.4.6.

Froelich, P.N., 1980. Analysis of organic carbon in marine sediments. Limnol. Oceanogr. 25, 564–572. https://doi.org/10.4319/lo.1980.25.3.0564.

Frost, R.L., Martens, W.N., Hales, M.C., 2009. Thermogravimetric analysis of selected group II carbonate minerals —implication for the geosequestration of greenhouse gases. J. Therm. Anal. Calorim. 95, 999–1005. https://doi.org/10.1007/s10973-008-9196-7.

Fuss, S., Lamb, W.F., Callaghan, M.W., Hilaire, J., Creutzig, F., Amann, T., Beringer, T., de Oliveira Garcia, W., Hartmann, J., Khanna, T., Luderer, G., Nemet, G.F., Rogelj, J., Smith, P., Vicente, J.L.V., Wilcox, J., del Mar Zamora Dominguez, M., Minx, J.C., 2018. Negative emissions – Part 2: costs, potentials and side effects. Environ. Res. Lett. 13, 063002 https://doi.org/10.1088/1748-9326/aabf9f.

Gale, A., Dalton, C.A., Langmuir, C.H., Su, Y., Schilling, J.-G., 2013. The mean composition of ocean ridge basalts. G-cubed 14, 489–518. https://doi.org/10.1029/2012GC004334.

Garcia, M.O., Hellebrand, E., 2020. Celestine discovered in Hawaiian basalts. Am. Mineral. 105, 52–57. https://doi.org/10.2138/am-2020-6995.

Gillespie, M.R., Styles, M.T., 1999. BGS Rock Classification Scheme, Volume 1, Classification of Igneous Rocks. British Geological Survey Research Report, second ed. RR 99–06.

Gislason, S.R., Arnorsson, S., Armannsson, H., 1996. Chemical weathering of basalt in Southwest Iceland; effects of runoff, age of rocks and vegetative/glacial cover. Am. J. Sci. 296, 837–907. https://doi.org/10.2475/ajs.296.8.837.

Guo, F., Wu, F., Mu, Y., Hu, Y., Zhao, X., Meng, W., Giesy, J.P., Lin, Y., 2016. Characterisation of organic matter of plants from lakes by thermal analysis in a N_2 atmosphere. Nature Sci. Rep. 6, 22877 https://doi.org/10.1038/srep22877.

Haines, P.J., 2002. Principles of Thermal Analysis and Calorimetry. The Royal Society of Chemistry, p. 320. https://doi.org/10.1039/9781847551764.

Hartmann, J., West, A.J., Renforth, P., Kohler, P., De La Rocha, C.L., Wolf-Gladrow, D.A., Durr, H.H., Scheffran, J., 2013. Enhanced chemical weathering as a geoengineering strategy to reduce atmospheric carbon dioxide, supply nutrients, and mitigate ocean acidification. Rev. Geophys. 51, 113–149. https://doi.org/10.1002/rog.20004.

Hernández-Uribe, D., Palin, R.M., Cone, K.A., Cao, W., 2020. Petrological implications of seafloor hydrothermal alteration of subducted mid-ocean ridge basalt. J. Petrol. 61. https://doi-org.eres.qnl.qa/10.1093/petrology/egaa086.

Hill, J.O., 1991. For better thermal analysis and calorimetry. In: International Confederation for Thermal Analysis (ICTA), third ed. Newcastle, Australia.

Hövelmann, J., Putnis, A., Geisler, T., Schmidt, B.C., Golla-Schindler, U., 2010. The replacement of plagioclase feldspars by albite: observations from hydrothermal experiments. Contrib. Mineral. Petrol. 159, 43–59. https://doi.org/10.1007/s00410-009-0415-4.

IPCC. 2014. Climate Change 2014: Mitigation of Climate Change. Contribution of Working Group III to the Fifth Assessment Report of the Intergovernmental Panel on Climate Change Ed O.R. Edenhofer et al. (Cambridge: Cambridge University Press) Summary for policymakers.

IPCC, 2021. Summary for policymakers. In: Masson-Delmotte, V., Zhai, P., Pirani, A., Connors, S.L., Péan, C., Berger, S., Caud, N., Chen, Y., Goldfarb, L., Gomis, M.I., Huang, M., Leitzell, K., Lonnoy, E., Matthews, J.B.R., Maycock, T.K., Waterfield, T., Yelekçi, O., Yu, R., Zhou, B. (Eds.), Climate Change 2021: the Physical Science Basis. Contribution of Working Group I to the Sixth Assessment Report of the Intergovernmental Panel on Climate Change. Cambridge University Press.

Kanakiya, S., Adam, L., Esteban, L., Rowe, M.C., Shane, P., 2017. Dissolution and secondary mineral precipitation in basalts due to reactions with carbonic acid. J. Geophys. Res. Solid Earth 122, 4312–4327. https://doi.org/10.1002/2017JB014019.

Kantola, I.B., Masters, M.D., Beerling, D.J., Long, S.P., DeLucia, E.H., 2017. Potential of global croplands and bioenergy crops for climate change mitigation through deployment for enhanced weathering. Biol. Lett. 13, 20160714 https://doi.org/10.1098/rsbl.2016.0714.

Kelland, M.E., Wade, P.W., Lewis, A.L., Taylor, L.L., Sarkar, B., Andrews, M.G., Lomas, M.R., Cotton, T.E.A., Kemp, S.J., James, R.H., Pearce, C.R., Hartley, S.E., Hodson, M.E., Leake, J.R., Banwart, S.A., Beerling, D.J., 2020. Increased yield and CO_2 sequestration potential with the C4 Cereal Sorghum Bicolor cultivated in basaltic rock dust-amended agricultural soil. Global Change Biol. 26, 3658–3676. https://doi.org/10.1111/gcb.15089.

Kemp, S.J., Wagner, D., Mounteney, I., 2010. Low Level Detection and Quantification of Carbonate Species Using Thermogravimetric and Differential Thermal Analysis. British Geological Survey Internal Report. IR/09/074.

Kemp, S.J., Smith, F.W., Wagner, D., Mounteney, I., Bell, C.P., Milne, C.J., Gowing, C.J. B., Pottas, T.L., 2016. An improved approach to characterise potash-bearing evaporite deposits, evidenced in North Yorkshire, UK. Econ. Geol. 111, 719–742. https://doi.org/10.2113/econgeo.111.3.719.

Kirstein, L.A., Davies, G.R., Heeremans, M., 2006. The petrogenesis of Carboniferous–Permian dyke and sill intrusions across northern Europe. Contrib. Mineral. Petrol. 152, 721–742. https://doi:10.1007/s00410-006-0129-9.

Kohler, P., Hartmann, J., Wolf-Gladrow, D.A., 2010. Geoengineering potential of artificially enhanced silicate weathering of olivine. Proceedings of the National Academy of Sciences of the United States of America 107. https://doi.org/10.1073/pnas.1000545107, 20 228–20 233.

Kumar, A., Shrivastava, J., 2019. Thermodynamic modelling and experimental validation of CO_2 mineral sequestration in mandla basalt of the Eastern Deccan volcanic province, India. J. Geol. Soc. India 93, 269–277. https://doi.org/10.1007/s12594-019-1173-1.

Lavoie, D., 1995. Carbonate botryoids in Lower Devonian amygdaloidal basalts; evidence for precipitation of high-magnesium calcite from heated and volcanic CO2-buffered marine waters. J. Sediment. Res. 65, 541–546. https://doi.org/10.1306/d4268121-2b26-11d7-8648000102c1865d.

Le Bas J., M., Le Maitre W., R., Streckeisen, A., Zanettin, B., 1986. A Chemical Classification of Volcanic Rocks Based on the Total Alkali-Silica Diagram. J. Petrol. 27, 745–750. https://doi.org/10.1093/petrology/27.3.745.

Le Bas, M.J., Streckeisen, A.L., 1991. The IUGS systematics of igneous rocks. J. Geol. Soc. 148, 825–833. https://doi.org/10.1144/gsjgs.148.5.0825.

Lefebvre, D., Goglio, P., Williams, A., Manning, D.A.C., de Azevedo, C., Bergmann, M., Meersmans, J., Smith, P., 2019. Assessing the potential of soil carbonation and enhanced weathering through Life Cycle Assessment: a case study for Sao Paulo State, Brazil. J. Clean. Prod. 233, 468–481. https://doi.org/10.1016/j.jclepro.2019.06.099.

Lewis, A.L., Wade, P.W., Kemp, S.J., Hodson, M.E., Taylor, L.L., Sarkar, B., Yeong, B., James, R.H., Pearce, C.R., Davies, K., Nelson, P., Bird, M., Kantola, I., Masters, M., DeLucia, E., Leake, J.R., Banwart, S.A., Beerling, D.J., 2021. Effects of mineralogy, chemistry and physical properties of basalts on carbon capture potential and elemental plant-nutrient release via enhanced weathering. Appl. Geochem. 132 https://doi.org/10.1016/j.apgeochem.2021.105023.

Li, G., Hartmann, J., Derry, L.A., West, A.J., You, C.-F., Long, X., Zhang, T., Li, L., Li, G., Qiu, W., Li, T., Liu, L., Chen, Y., Ji, J., Zhao, L., Chen, J., 2016. Temperature dependence of basalt weathering. Earth Planet Sci. Lett. 443, 59–69. https://10.1016/j.epsl.2016.03.015.

Liu, P., Wang, X., Horita, J., Fang, X., Zheng, J., Li, X., Meng, Q., 2019. Evaluation of total organic carbon contents in carbonate source rocks by modified acid treatment method and the geological significance of acid-soluble organic matters. Energy Explor. Exploit. 37, 219–229. https://doi.org/10.1177/0144598718786034.

Lopez-Capel, E., Sohi, S.P., Gaunt, J.L., Manning, D., 2005. A. Use of thermogravimetry-differential scanning calorimetry to characterize modelable soil organic matter fractions. Soil Sci. Soc. Am. J. 69, 136–140. https://doi.org/10.2136/sssaj2005.0136a.

MacDonald, J.M., Faithfull, J.W., Roberts, N.M.W., Davies, A.J., Holdsworth, C.M., Newton, M., Williamson, S., Boyce, A., John, C.M., 2019. Clumped-isotope palaeothermometry and LA-ICP-MS U–Pb dating of lava-pile hydrothermal calcite veins. Contrib. Mineral. Petrol. 174, 63. https://doi.org/10.1007/s00410-019-1599-x.

MacDougall, D., Crummett, W.B., 1980. Guidelines for data acquisition and data quality evaluation in environmental chemistry. Anal. Chem. 52, 2242–2249. https://doi.org/10.1021/ac50064a004.

Mahoney, C., März, C., Buckman, J., Wagner, T., Blanco-Velandia, V.-O., 2019. Pyrite oxidation in shales: implications for palaeo-redox proxies based on geochemical and SEM-EDX evidence. Sediment. Geol. 389, 186–199. https://doi.org/10.1016/j.sedgeo.2019.06.006.

Manning, D.A.C., Lopez-Capel, E., Barker, S., 2005. Seeing soil carbon: use of thermal analysis in the characterization of soil C reservoirs of differing stability. Mineral. Mag. **69**, 425–435. https://doi.org/10.1180/0026461056940260.

Marini, L., 2007. Geological Sequestration of Carbon Dioxide: Thermodynamics, Kinetics, and Reaction Path Modeling. Elsevier, Amsterdam, p. 470.

McGrail, B.P., Schaef, H.T., Ho, A.M., Chien, Y.J., Dooley, J.J., Davidson, C.L., 2006. Potential for carbon dioxide sequestration in flood basalts. J. Geophys. Res. 111, B12201 https://doi.org/10.1029/2005JB004169.

Meixner, H., 1964. 212. Strontianit aus dem Basalt vom Pauliberg, Burgenland. Carinthia II. In: Meixner, H. (Ed.), Neue Mineralfunde in Den Österreichischen Ostalpen XIX, 154/74, pp. 19–21.

Mercure, J.-F., Pollitt, H., Viñuales, J.E., Edwards, N.R., Holden, P.B., Chewpreecha, U., Salas, P., Sognnaes, I., Lam, A., Knobloch, F., 2018. Macroeconomic impact of stranded fossil fuel assets. Nat. Clim. Change 8, 558–593. https://doi.org/10.1038/s41558-018-0182-1.

Milodowski, A.E., Morgan, D.J., 1980. Identification and estimation of carbonate minerals at low-levels by evolved CO_2 analysis. Nature 286, 248–249. https://doi.org/10.1038/286248a0.

Minx, J.C., Lamb, W.F., Callaghan, M.W., Bornmann, L., Fuss, S., 2017. Fast growing research on negative emissions. Environ. Res. Lett. 12, 035007 https://doi.org/10.1088/1748-9326/aa5ee5.

Minx, J.C., Lamb, W.F., Callaghan, M.W., Fuss, S., Hilaire, J., Creutzig, F., Amann, T., Beringer, T., de Oliveira Garcia, W., Hartmann, J., Khanna, T., Lenzi, D., Luderer, G., Nemet, G.F., Rogelj, J., Smith, P., Vicente, J.L., Wilcox, J., del Mar Zamora Dominguez, M., 2018. Negative emissions – Part 1: research landscape and synthesis. Environ. Res. Lett. 13, 063001 https://doi.org/10.1088/1748-9326/aabf9b.

Möller, P., Rosenthal, E., Inbar, N., Magri, F., 2016. Hydrochemical considerations for identifying water from basaltic aquifers: the Israeli experience. J. Hydrol.: Reg. Stud. 5, 33–47. https://doi.org/10.1016/j.ejrh.2015.11.016.

Morgan, D.J., 1971. The dissociation of strontianite and its quantitative estimation by thermogravimetry. Thermal Analysis 3, 675–682. https://doi.org/10.1007/978-3-0348-5775-8_57.

Morgan, D.J., 1977. Simultaneous DTA-EGA of minerals and natural mineral mixtures. J. Therm. Anal. 12, 245–263. https://doi.org/10.1007/BF01909481.

Morgan, D.J., Warrington, S.B., Warne, S.S.T.J., 1988. Earth sciences applications of evolved gas-analysis - a review. Thermochim. Acta 135, 207–212. https://doi.org/10.1016/0040-6031(88)87387-8.

Mu, J., Perlmutter, D.D., 1981. Thermal decomposition of carbonates, carboxylates, oxalates, acetates, formats, and hydroxides. Thermochim. Acta 49, 207–218.

Myhre, G., Shindell, D., Bréon, F., Collins, W., Fuglestvedt, J., Huang, J., et al., 2013. Anthropogenic and natural radiative forcing. In: Stocker, T.F., Qin, D., Plattner, G.-K., Tignor, M., Allen, J., Boschung, J., et al. (Eds.), Climate Change 2013: the Physical Science Basis. Contribution of Working Group I to the Fifth Assessment Report of the Intergovernmental Panel on Climate Change. Cambridge University Press, Cambridge; New York, NY, pp. 658–740. https://doi.org/10.1017/CBO9781107415324.018.

Nemet, G.F., Callaghan, M.W., Creutzig, F., Fuss, S., Hartmann, J., Hilaire, J., Lamb, W. F., Minx, J.C., Rogers, S., Smith, P., 2018. Negative emissions – Part 3: innovation and upscaling. Environ. Res. Lett. 13 https://doi.org/10.1088/1748-9326/aabff4.

Oelkers, E.H., Gislason, S.R., Matter, J., 2008. Mineral carbonation of CO_2. Elements 4, 331–335. https://doi.org/10.2113/gselements.4.5.333.

Otsuka, R., 1986. Recent studies on the decomposition of the dolomite group by thermal analysis. Thermochim. Acta 100, 69–80. https://doi.org/10.1016/0040-6031(86)87051-4.

Otterns, B., Götze, J., Schuster, R., Krenn, K., Hauzenburger, C., Zsolt, B., Vennemann, T., 2019. Exceptional multi stage mineralization of secondary minerals in cavities of flood basalts from the Deccan Volcanic Province, India. Minerals 9, 1–41. https://doi.org/10.3390/min9060351.

Palandri, J.L., Kharaka, Y.K., 2004. A Compilation of Rate Parameters of Water-Mineral Interaction Kinetics for Application to Geochemical Modelling. US Geological Survey Open File Report. https://doi.org/10.3133/ofr20041068, 2004-1068.

Parsons, A.J., Inglethorpe, S.D.J., Morgan, D.J., Dunham, A.C., 1997. Evolved gas analysis (EGA) of brick clays. J. Therm. Anal. 48, 49–62. https://doi.org/10.1007/BF01978965.

Peng, C., Anabaraonye, B., Crawshaw, J.P., Maitland, G.C., Trusler, M., 2016. FDCCS16 Kinetics of carbonate mineral dissolution in CO_2-acidified brines at storage reservoir conditions. Faraday Discuss 192. https://doi.org/10.1039/C6FD00048G.

Pillot, D., Deville, E., Prinzhofer, A., 2014. Identification and quantification of carbonate species using Rock-Eval pyrolysis. Oil Gas Sci. Technol. 69, 341–349. https://10.2516/ogst/2012036.

Pogge von Strandmann, P.A.E., Burton, K.W., Snaebjörnsdottir, S.O., Sigfússon, B., Aradóttir, E.S., Gunnarsson, I., Alfredsson, H.A., Mesfin, K.G., Oelkers, E.H., Gislason, S.R., 2019. Rapid CO_2 mineralisation into calcite at the CarbFix storage site quantified using calcium isotopes. Nat. Commun. 10, 1983. https://doi.org/10.1038/s41467-019-10003-8.

Raja, P.M.V., Barron, A.R., 2020. Physicals Methods in Chemistry and Nano Science. Connections, Rice University, p. 702.

Robinson, T., Bronson, B., Gogolek, P., Mehrani, P., 2016. Sample preparation for thermo-gravimetric determination and thermo-gravimetric characterization of refuse derived fuel. Waste Manag. 48, 265–274. https://doi.org/10.1016/j.wasman.2015.11.018.

Rockström, J., Gaffney, O., Rogelj, J., Meinshausen, M., Nakicenovic, N., Schellnhuber, H.J., 2017. A roadmap for rapid decarbonization. Science 355, 1269–1271. https://doi.org/10.1126/science.aah3443.

Rodriguez-Navarro, C., Ruiz-Aguido, E., Luque, A., Rodriguez-Navarro, A.B., Ortega-Huertas, M., 2009. Thermal decomposition of calcite: mechanisms of formation and

textural evolution of CaO nanocrystals. Am. Mineral. 94, 578–593. https://doi.org/10.2138/am.2009.3021.
Rosenbauer, R.J., Thomas, B., Bischoff, J.L., Palandri, J., 2012. Carbon sequestration via reaction with basaltic rocks: geochemical modeling and experimental results. Geochem. Cosmochim. Acta 89, 116–133. https://doi.org/10.1016/j.gca.2012.04.042.
Sabine, P.A., Morey, J.E., Shergold, F.A., 1954. The correlation of the mechanical properties and petrography of a series of quartz-dolerite roadstones. J. Appl. Chem. 4, 131–137. https://doi.org/10.1002/jctb.5010040307.
Sayyed, M.R.G., 2014. Flood basalt hosted palaeosols: potential palaeoclimatic indicators of global climate change. Geosci. Front. 5, 791–799. https://doi.org/10.1016/j.gsf.2013.08.005.
Schaef, H.T., McGrail, B.P., Owen, A.T., 2009. Basalt-CO_2-H_2O interactions and variability in carbonate mineralization rates. Energy Proc. 1, 4899–4906. https://doi.org/10.1016/j.egypro.2009.02.320.
Schumacher, B.A., 2002. Methods for the Determination of Total Organic Carbon (TOC) in Soils and Sediments. US EPA Report NCEA-. *C-1282*.
Seyfried, W.E., Bischoff, J.L., 1974. Low temperature basalt alteration by sea water: an experimental study at 70°C and 150°C. Geochem. Cosmochim. Acta 43, 1937–1947. https://doi.org/10.1016/0016-7037(79)90006-1.
Shahraki, B.K., Mehrabi, B., Dabiri, R., 2009. Thermal behaviour of Zefreh dolomite mine (Central Iran). J. Min. Metall. B Metall. 45, 35–44. https://doi.org/10.2298/JMMB0901035S.
Shelley, D., 1992. Igneous and Metamorphic Rocks under the Microscope. Classification, Textures, Microstructures and Mineral Preferred Orientations. Chapman and Hall, London.
Sissmann, O., Brunet, F., Martinez, I., Guyot, F., Verlaguet, A., Pinquier, Y., Duval, D., 2014. Enhanced olivine carbonation within a basalt as compared to single-phase experiments: re-evaluating the potential of CO_2 mineral sequestration. Environ. Sci. Technol. 48, 5512–5519. https://doi.org/10.1021/es405508a.
Smith, G.A., Hayman, G.A., 1987. Geologic Map of the Eagle Butte and Gateway Quadrangles, Jefferson and Wasco Counties. Oregon: Oregon Department of Geology and Mineral Industries, Geological Map Series GMS-43. scale 1:24,000.
Smith, P., Adams, J., Beerling, D.J., Beringer, T., Calvin, K.V., Fuss, S., Griscom, B., Hagemann, N., Kammann, C., Kraxner, F., Minx, J.C., Popp, A., Renforth, P., Vicente, J.L., Keesstra, S., 2019. Land-management options for greenhouse gas removal and their impacts on ecosystem services and the sustainable development Goals. Annu. Rev. Environ. Resour. 44, 255–286. https://doi.org/10.1146/annurev-environ-101718-033129.
Smykatz-Kloss, W., 1974. Differential Thermal Analysis: Application and Results in Mineralogy. Springer Verlag. https://doi.org/10.1007/978-3-642-65951-5. Berlin, Heidelberg, New York.
Streckeisen, A., 1974. Classification and Nomenclature of Plutonic Rocks. Geologische Rundschau 63, 773–786. https://doi.org/10.1007/BF01820841.
Strefler, J., Amann, T., Bauer, N., Kriegler, E., Hartmann, J., 2018. Potential and costs of carbon dioxide removal by enhanced weathering of rocks. Environ. Res. Lett. 13, 034010 https://doi.org/10.1088/1748-9326/aaa9c4.
Sutter, B., Boynton, W.V., Ming, D.W., Niles, P.B., Morris, R.V., Golden, D.C., Lauer, H.V., Fellows, C., Hamara, D.K., Mertzman, S.A., 2012. The detection of carbonate in the Martian soil at the Phoenix landing site: a laboratory investigation and comparison with the thermal and evolved gas analyzer (TEGA) data. Icarus 218, 290–296. https://doi.org/10.1016/j.icarus.2011.12.002.
Sutter, B., McAdam, A.C., Mahaffy, P.R., Ming, D.W., Edgett, K.S., Rampe, E.B., Eigenbrode, J.L., Franz, H.B., Freissinet, C., Grotzinger, J.P., Steele, A., House, C.H., Archer, P.D., Malespin, C.A., Navarro-Gonzalez, R., Stern, J.C., Bell, J.F., Calef, F.J., Gellert, R., Glavin, D.P., Thompson, L.M., Yen, A.S., 2017. Evolved gas analyses of sedimentary rocks and eolian sediment in Gale Crater, Mars: results of Curiosity rover's sample analysis at Mars instrument from Yellowknife Bay to the Namib Dune. J. Geophys. Res.: Planets 122, 2574–2609. https://doi.org/10.1002/2016JE005225.
Swoboda, P., Döring, T.F., Hamer, M., 2022. Remineralizing Soils? The agricultural usage of silicate rock powders: a review. Sci. Total Environ. 807, 150976 https://doi.org/10.1016/j.scitotenv.2021.150976.
Tahir, S., Musta, B., Rahim, I.R., 2010. Geological heritage features of Tawau volcanic sequence, Sabah. Bull. Geol. Soc. Malays. 56, 79–85. https://doi.org/10.7186/bgsm56201012.
Taylor, L.L., Leake, J.R., Quirk, J., Hardy, K., Banwart, S.A., Beerling, D.J., 2009. Biological weathering and the long-term carbon cycle: integrating mycorrhizal evolution and function into the current paradigm. Geobiology 7, 171–191. https://doi.org/10.1111/j.1472-4669.2009.00194.x.
Taylor, L.L., Quirk, J., Thorley, R.M.S., Kharecha, P.A., Hansen, J., Ridgwell, A., Lomas, M.R., Banwart, S.A., Beerling, D.J., 2016. Enhanced weathering strategies for stabilizing climate and averting ocean acidification. Nat. Clim. Change 6, 402–406. https://doi.org/10.1038/nclimate2882.
The Royal Society and Royal Academy of Engineering, 2018. Greenhouse Gas Removal. Retrieved from. https://royalsociety.org/~/media/policy/projects/greenhouse-gas-removal/royal-society-greenhouse-gas-removal-report-2018.pdf.
United Nations Framework Convention on Climate Change, 2015. Adoption of the Paris Agreement: Proposal by the President to the United Nations Framework Convention on Climate Change. United Nations Framework Convention on Climate Change.
USGS, 2015. Basalt". USGS volcano hazards program – glossary. USGS, 8 April 2015. Retrieved 13 February 2020.
USGS, 2019. Catoctin Formation - Metabasalt [WWW Document]. https://mrdata.usgs.gov/geology/state/sgmc-unit.php?unit=VACAZc%3B0.
Vakilifard, N., Kantzas, E.P., Edwards, N.R., Holden, P.B., Beerling, D.J., 2021. The role of enhanced rock weathering deployment with agriculture in limiting future warming and protecting coral reefs. Environ. Res. Lett. 19, 094005 https://doi.org/10.1088/1748-9326/ac1818.
Wang, X., Wang, J., Zhang, J., 2012. Comparisons of three methods for organic and inorganic carbon in calcareous soils of Northwestern China. PLoS One 7, e44334. https://doi.org/10.1371/journal.pone.0044334.
Warne, S.S.T.J., 1977. Carbonate mineral detection by variable atmosphere differential thermal analysis. Nature 269, 678. https://doi.org/10.1038/269678a0.
Warne, S.S.T.J., 1986. Applications of variable atmosphere DTA (in CO_2) to improved detection and content evaluation of anhydrous carbonates in mixtures. Thermochim. Acta 109, 243–252. https://doi.org/10.1016/0040-6031(86)85025-0.
Warne, S.S.T.J., Mitchell, B.D., 1979. Variable atmosphere DTA in identification and determination of anhydrous carbonate minerals in soils. J. Soil Sci. 30, 111–116. https://doi.org/10.1111/j.1365-2389.1979.tb00969.x.
Weliky, K., Suess, E., André Ungerer, C., Müller, P.J., Fischer, K., 1983. Problems with accurate carbon measurements in marine sediments and particulate matter in seawater: a new approach. Limnol. Oceanogr. 25, 1252–1259. https://doi.org/10.4319/lo.1983.28.6.1252.
Whitehead, P.W., Stephenson, P.J., McDougall, I., Hopkins, M.S., Graham, A.W., Collerson, K.D., Johnson, D.P., 2007. Temporal development of the Atherton basalt province, north Queensland. Aust. J. Earth Sci. 54, 691–709. https://doi.org/10.1080/08120090701305236.
Wolff-Boenisch, D., Gislason, S.R., Oelkers, E.H., 2006. The effect of crystallinity on dissolution rates and CO_2 consumption capacity of silicates. Geochem. Cosmochim. Acta 70, 858–870. https://doi.org/10.1016/j.gca.2005.10.016.
Wright, A.F., Bailey, J.S., 2001. Organic carbon, total carbon, and total nitrogen determinations in soils of variable calcium carbonate contents using a Leco CN-2000 Dry Combustion Analyzer. Commun. Soil Sci. Plant Anal. 32, 3243–3258. https://doi.org/10.1081/CSS-120001118.
Zhang, G.-L., Smith-Duque, C., 2014. Seafloor basalt alteration and chemical change in the ultra thinly sedimented South Pacific. G-cubed 15, 3066–3080. https://doi.org/10.1002/2013GC005141.